Last Glacial Maximum and early deglaciation in the Stura Valley, southwestern European Alps

Adriano Ribolini[1], Matteo Spagnolo[2], Andrew J. Cyr[3], Paolo Roberto Federici[4]

[1] Department of Earth Sciences, University of Pisa, Italy

[2] Department of Geography & Environment, University of Aberdeen, UK

[3] U.S. Geological Survey, Geology, Minerals, Energy, and Geophysics Science Center, Moffett Field, CA, USA

[4] Retired, former Department of Earth Sciences, University of Pisa, Italy

Abstract:

We combined data from geomorphologic surveys, glacial modelling, and ^{10}Be exposure ages of boulders on moraines, to investigate the Last Glacial Maximum (LGM) and the early retreat glacial phases in the Stura Valley of the Maritime Alps. We used the exposure ages to reconstruct the timing of standstills or readvances which interrupted the post-LGM withdrawal, initiated ~24 ka. We mapped and dated the frontal moraines of a first glacial standstill/readvance at a short distance (~ 7 km) from the maximum external limit of the LGM, which occurred at ~22 ka, and a second one at ~19 ka (Bühl stadial). This morpho-chronologic succession is congruent with that obtained in the adjacent Gesso Valley and, combined with the similarity of Equilibrium Line Altitude values, demonstrates a consistent glacial response in the Maritime Alps to climatic forcing.

Our data are chronologically consistent with those of the southern flank of the European Alps, stressing not only a general synchroneity of the LGM across the various sectors, but also that of a LGM recessional standstill or readvance at ~22 ka. The short distance between the LGM moraines and the recessionary phase moraines indicates a modest variation in the mass balance of the Maritime Alps glaciers during this time interval. A similar modest variation between LGM and the first recessional phase glacier mass balance is also found throughout the western sector of the Southern Alps but is considerably more pronounced for the glaciers of the central-eastern sectors. This behaviour can be explained by the interplay between the moisture supplied by southern currents sourced in the Western Mediterranean and that advected by the westerlies sourced in the North Atlantic, which affected the various sectors of the Southern Alps differently.

Keywords: Last Glacial Maximum, glacial retreat, cosmogenic exposure ages, Equilibrium Line Altitude, Maritime Alps

Introduction

During the Last Glacial Maximum (LGM), around 18-24 ka BP (Hughes et al. 2013; Hughes and Gibbard, 2015 and references therein), the European Alps were covered by ice caps and large valley glaciers (Ehlers and Gibbard 2004; Ivy-Ochs et al. 2008; Ehlers et al., 2011). Some illustrations of the extent of this glacial landscape exist in the literature, from the pioneering regional reconstructions at the beginning of the 20th century (Penck and Brückner, 1901-1909; Dainelli, 1939; Castiglioni, 1940) to the modern ones (van Husen, 1987; Ehlers and Gibbard, 2004; Geologische Bundesanstalt, 2013), including those generated by glacial modelling (Becker et al., 2016; Seguinot et al., 2018). However, all these reconstructions suffer from inaccuracy in the Maritime Alps, at the southwestern limit of the Alpine chain, where the extent of reconstructed glaciers is often at odds with field evidence (Fig. 1 a, b). This may be due to both the scarcity of geomorphologic/chronologic data in this region that, until recently, consisted solely of observations from the early-mid 20th century, and to the idea that the proximity to the Mediterranean Sea would have resulted in only modest development of glaciers in this sector of the Alps (Fig. 1c).

With the exception of the Maritime Alps, which remain amongst the least investigated sector of the European Alps, the termini of LGM glaciers draining the southern slope of the Alps (Southern Alps hereafter) and overlooking the Po River Plain are well defined in the western (Rivoli-Avigliana, Ivrea, Lake Orta, Lake Verbano end moraines/amphitheatres), central (Lake Garda moraine amphitheatre) and eastern (Vittorio Veneto and Tagliamento moraine/end moraine/amphitheatres) sectors of the Alpine chain (Bini et al., 2004; 2009; 2014; Kelly et al., 2004; Pellegrini et al., 2005; Monegato et al., 2007;2017; Gianotti et al., 2008; Forno et al., 2010; Ivy-Ochs et al., 2018; Braakhekke et al., 2020; Kamleitner et al., 2022). The robust chronology of these deposits, largely based on cosmogenic nuclide geochronology (Ivy-Ochs et al., 2018; Kamleitner et al., 2022 and references therein), reveals that these glacial expansions most likely represent a synchronous response to cold conditions and an altered atmospheric circulation, dominated by the southern shift of the polar front and the jet stream in the North Atlantic (Monegato et al., 2017).

The only palaeoglacial reconstruction available for the Maritime Alps, the Gesso Valley Glacier, suggests that, unlike all other Alpine sectors mentioned above, LGM glaciers did not reach the piedmont (Po River) plain in this sector of the Alps (Federici et al., 2012; Federici et al., 2017). However, the Gesso Valley was not the largest valley system in the area, and more data are needed from neighbouring valleys to confirm the regional scale of such a scenario and to investigate the reasons for a potentially limited LGM glacier extent in the Maritime Alps.

During the post-LGM deglaciation, a series of glacial readvances across the Alps characterized the Lateglacial period (19.0-11.7 ka) (i.e., the Termination I (Ivy-Ochs et al. 2008; Reitner, 2007) preceding the onset of the Holocene. Numerous cosmogenic nuclide surface exposure ages of frontal moraines demonstrate a consistent timing of these glacial readvances across the Alps, strengthening the Alpine Stadial chronology and elucidating the link between climatic events and Alpine glacier readvances (Ivy-Ochs et al., 2008; 2015; Federici et al. 2017; Rea at al. 2020). A five-fold Lateglacial stratigraphy for the Alps is commonly accepted: from older to younger the Bühl, Gschnitz, Clavadel/Sender, Daun and Egesen stadials (Ivy-Ochs et al., 2008). The ages of the Bühl and Gschnitz stadials partly fall in the Oldest Dryas cold period (~18-14.6 ka, the GS2-1a stadial in the Greenland chronology), whereas the Older Dryas (~14.0-13.9 ka, the GI-1d stadial in the Greenland chronology) and the Younger Dryas (~12,.9-11.7 ka, the GS1 stadial in the Greenland chronology)) cold events were responsible for the Clavadel/Sender, Daun and Egesen stadials, (Ivy-Ochs et al., 2008; Loewe et al., 2008; Lotter et al., 2012; Rasmussen et al., 2014; ~~Carlson and Winsor, 2019;~~ Cheng et al., 2020). Like for the LGM, the Lateglacial palaeoglaciologic and chronologic data for the Maritime Alps are sparse relative to other sectors of the Alps, with a few notable exceptions (Federici et al., 2008; 2012; 2017; Rolland et al., 2020; Spagnolo and Ribolini, 2019) (Fig. 2).

The limited availability of chronologically- and geomorphologically-constrained LGM to Lateglacial glacier advances in the Maritime Alps can lead to inaccurate reconstructions of glacial extent, more poorly constrained glacial models, and less robust palaeoclimatic inferences for the Alps.

In this paper we present the reconstruction and chronology of the extension of the LGM and early Lateglacial glaciers in the Stura di Demonte Valley (Stura Valley hereafter in the text), which is the largest drainage basin of the eastern flank (facing the Po plain) of the Maritime Alps (Fig. 1c). New Equilibrium Line of Altitude (ELA) and surface exposure ages of boulders on terminal moraines were calculated to support the geomorphological and sedimentological evidence. Finally, we use the combined reconstructions of palaeoglaciers in the Stura and Gesso valleys during the LGM and earliest phases of Lateglacial retreat to discuss similarities and differences between the Maritime Alps and other sectors of the Southern Alps and the implications for regional palaeoclimatic reconstructions.

Regional context

The Stura Valley drains the eastern side of the Maritime Alps, which are the southernmost portion of the European Alps (latitude of 43.9‑44.4° N; longitude of 6.9‑7.6° E) (Fig. 1c). This alpine region is very close (40‑60 km) to the Mediterranean Sea (hence the term “Maritime”), with elevations exceeding 3,000 m above sea level (a.s.l.), and where small glaciers still survive.

The Stura Valley encompasses approximately 590 km^2 and its elevation ranges from ~3,000 m a.s.l. at the watershed divide to 580 m a.s.l., where it terminates into the upper Po Plain (locally known as Cuneo Plain) (Fig. 1c). In the upper half of its extent, the valley exhibits a NW-SE oriented axis, parallel to the major tectonic elements and the structural axis of the crystalline bedrock (Perello and Piana, 1997; Ribolini, 2000; Musumeci et alii 2003; Ribolini and Spagnolo, 2008; Bonetto et al., 2017; Marrucci et al., 2018). In the lower half, the valley has a clear W-E direction, cross-cutting the main geological structures (Marrucci et al., 2018). The valley geometry exposes bedrock consisting of crystalline rocks (high-grade metamorphic and granitoid rocks) for most of the right (S-SW) side, and sedimentary rocks (quartzites, limestones, dolomites and sandstone flysch series) for most of the left (N-NE) side (Malaroda et al., 1970). However, the lowermost part of the valley, where the glacial deposits investigated in the present study are found, is characterised by sedimentary rocks only. This is important as it means that the lithological composition of boulders/pebbles could aid the glacial interpretation of some landforms in this portion of the valley.

The geomorphology of the Stura Valley has not received particular attention to date. However, the valley experienced intense glacial erosion which resulted in a U-shaped cross-profile in many sections. The Quaternary glacial depositional processes left important accumulations of till, locally shaped as lateral and frontal moraines. These have been attributed to both the LGM and cold periods of the Lateglacial (Malaroda et al., 1970; Spagnolo, 2007; Federici, 2012) but, with two exceptions (Ribolini et al., 2007; Spagnolo and Ribolini, 2019), no chronologic constraints are available to confirm these early interpretations. Permafrost creeping has formed numerous rock glaciers, currently active at elevations above 2,300-2,400 m a.s.l. (Ribolini and Fabre, 2006; Ribolini et al. ; 2007; 2010). Fluvial processes, with a minor contribution of sediment from debris flows and landslides, often generated in paraglacial deposits from steep valley flanks, are currently the dominant geomorphic processes, locally superimposed on and reworking glacial landforms (Spagnolo, 2007; Capitani and Marrucci, 2008).

As a result of their geographic position, the Maritime Alps are sensitive to climatic variations dominated by the interplay between the N-S oscillations of the polar front and the eastward atmospheric perturbations generated in the North Atlantic Ocean, along with cyclogenesis phenomena occurring in the northwestern Mediterranean (Stefanini and Ribolini, 2003; Federici et al. 2012). At 1,400 m a.s.l., present-day annual precipitation is generally lower than in the rest of the Alps (Federici et al., 2012; Isotta et al., 2014) and is bimodal, with peaks of ~160 mm in spring and ~250 mm in autumn. Snow cover depth at about 2,000 m a.s.l. increases regularly from November (>10 cm) to April (>280 cm), constantly exceeds 100 cm between December and April, and typically persists on the surface until early June (Ribolini and Fabre, 2007; Federici et al., 2012). The present-day (2001–2018) mean annual precipitation at about 2,000 m a.s.l is 1,487 mm/yr (Spagnolo and Ribolini, 2019). Temperatures peak at ~ 16 °C in summer, and are generally higher than in other, nearby Alpine regions (Federici et al., 2012; Durand et al., 2009). The mean annual air temperature ranges between 4.5 and 6.4 °C.

Methods

Geomorphology

We studied the geomorphology of the Stura Valley through various field surveys undertaken over the last decade. These investigations, subsequently augmented by high resolution remote sensing analysis (Quickbird satellite imagery, accessed via Google Earth in 2022), produced detailed geomorphological maps of the middle-lower valley, where a number of likely LGM to early Lateglacial glacial deposits were recognised, including the frontal moraines of Castelletto-Bedoira, Festiona and Bergemolo, which are the focus of this work (position of geomorphological sketch maps are reported in Fig. 1c). During our field surveys we also carried out observations of the stratigraphic composition and characteristics of the glacial deposits (structure, grain size, boulders/clasts lithology, weathering profile).

Palaeoglacier reconstruction and Equilibrium Line Altitude

We used a geographic information system (GIS) approach to semi-automatically reconstruct thickness and extent of the former glaciers that deposited the frontal moraines (Pellitero et al., 2016). The GIS tool creates a 3D glacier surface based on the lateral interpolation of a 2D glacier equilibrium profile, which is calculated by using a plastic rheology glacier model along user-defined flowlines (Benn and Hulton, 2010; Paterson, 1994; Shilling and Hollin, 1981). Glaciers are reconstructed by extrapolating the ice thickness along defined flowlines, after applying a default shear stress of 100 kPa and shape (F) factors to account for variation in the width of the glacial valley. The mapped glacial landforms (cirques, glacial valley steps, hanging valleys, lateral moraines) enabled us to constrain the reconstructions. The reconstructed 3D glacial surface was then used to calculate the Equilibrium Line Altitude (ELA) of the palaeoglaciers with a bespoke GIS tool (Pellitero et al., 2015), adopting an Accumulation Area Balance Ratio (AABR, Furbish and Andrews, 1984) of 1.6, which is consistent with other pan-Mediterranean ELA reconstructions (Rea, 2009; Ribolini et al., 2018; Spagnolo and Ribolini, 2019; Rea et al., 2020).

Cosmogenic ^{10}Be Exposure Geochronology

We sampled high-grade metamorphic boulders from moraines for surface exposure dating with ^{10}Be. On the Bedoira moraine, we collected samples from the tops of boulders that stand from 1 to 1.5 m above the surrounding moraine deposits and are between 2 and 3 m in diameter (Fig. 3a-c). On the Festiona moraine, we sampled from the tops of boulders that are 1.5 to 1.75 m above the surrounding moraine deposits and between 1.5 and 3 m in diameter (Fig. 3d-h). On the Bergemolo moraine, we sampled from the tops of boulders that stand 1.25 to 2.0 m above the surface of the moraine deposit and are between 2 and 3 m in diameter (Fig. 4). Where possible we restricted our sampling to the largest boulders residing on the moraine crest. In some cases (Bergemolo 1, Bedoira 2 and 3) boulders only occurred off of the crest; in these cases, we selected boulders as close to the moraine crest as possible, avoiding boulders with evidence of recent exhumation from within the moraine (e.g., differences in weathering, circum-boulder breaks in weathering rind). We collected samples from three boulders on each of the Bedoira and Bergemolo moraines, and samples of five boulders on the Festiona moraine (see also Fig. 5a,b and 6). Each sample was collected from a flat, though not necessarily horizontal, surface as far away from the boulder edges as possible. Samples were all <4-cm thick. We measured the inclination to the horizon at 30° intervals, as well as the strikes and dips of the sampled surfaces, in order to calculate the topographic- and self-shielding (Dunne et al., 1999).

Approximately 150 g of quartz were separated from each sample at Purdue University, West Lafayette, Indiana, USA, using methods modified from Kohl and Nishiizumi (1992). Following magnetic and gravimetric separation, and selective dissolution, the purified quartz was spiked with approximately 0.5 mg of ^{9}Be carrier solution prepared from beryl and dissolved in HF/HNO_3. After drying, fluorides were expelled with H_2SO_4. Iron was removed by anion exchange in 9 N HCl. Calcium, magnesium, some manganese, and alkali metals were removed during precipitation with NH_4OH. Beryllium was isolated from the resulting hydroxide gel by cation exchange in a 0.4 M oxalic acid solution (von Blanckenburg et al., 1996). Beryllium hydroxide was oxidized at 1100 °C, mixed with Nb, and packed into stainless steel holders for analysis by accelerator mass spectrometry (AMS).

AMS measurements of ^{10}Be/^{9}Be were made in 2007 at the Purdue Rare Isotope MEsurement (PRIME) Lab, Purdue University, against standards prepared by Kuni Nishiizumi (Nishiizumi et al., 2007). The values of these standards have been revised since the time of measurement (Nishiizumi et al., 2007); measurements have been adjusted to the new standardization. Sample shielding as a result of topography and the strike and dip of the sampled surfaces was calculated following Dunne et al. (1999). We calculated exposure ages using version 3 of the online calculator formerly known as the CRONUS-Earth online exposure age calculator (Balco et al., 2008; available at http://hess.ess.washington.edu/), following the Lifton-Sato-Dunai (Lifton et al., 2014) time-dependent magnetic field model scaled from a sea level-high latitude reference production rate of 3.92 atoms ^{10}Be per g of quartz (Borchers et al., 2016). Although we did not observe evidence for erosion of boulder surfaces, e.g. high intergranular relief, weathering pans, etc., in order to account for the effects of possible surface erosion, we calculated exposure ages for both 0 mm/kyr and 3 mm/kyr scenarios, where 3 mm/kyr is the typical maximum erosion rate applied to other surface exposure dates in the Alps (e.g., Ivy Ochs et al., 2006). We used the scripts built into the online calculator (Balco et al., 2008; available at http://hess.ess.washington.edu/) for detecting outliers and calculating mean ages of the moraines on which boulders reside. Outliers are identified by computing the p-value of the chi-squared statistic with respect to the mean, using the measurement uncertainty. If the p-value is not better than 0.01 then the measurement farthest away from the mean is removed; this process is repeated until there are fewer than three data remaining or half the data have been discarded, whichever comes first (documentation for version 3 of the online calculator formerly known as the CRONUS-Earth online exposure age calculator; http://hess.ess.washington.edu/). Sample information, individual boulder ages, and the mean and standard deviation of those ages for a given moraine are presented in Table 1 (Cyr et al., 2022).

Climate at the ELA

To estimate the climate condition at the ELAs of the reconstructed glacial phases, we used the empirical law that links annual precipitation (P_{ann} in mm) to melting season (summer in this instance) mean air temperature (T_{melt}) (Ohmura and Boettcher, 2018):

$$P_{ann}=5.87\ T_{melt}^{\ 2} + 230\ T_{melt} + 966 \quad (1)$$

We retrieved the temperature of the hottest month (T_{Jul}) from the analysis of chironomids (midges) preserved in sediments retrieved from a core in Lago della Costa, northern Italy (45° 16′ 13″ N, 11° 44′ 35″ E) (Samartin et al., 2016) for dates identified by our new ^{10}Be surface exposure ages (Table 1, Cyr et al., 2022). This site is about 350 km from the Stura Valley but no other chironomid series, or other palaeoclimatic proxies, extending to the LGM are available nearer to the Maritime Alps. In the absence of more specific proxy data, we used T_{Jul} as a proxy for T_{melt}. We applied a thermal lapse rate of 6.5°/1 km to adjust the chironomid-based T_{july} of the Lago della Costa to the elevation of Stura Valley ELAs.

Results

Geomorphology

In the mid-lower Stura Valley, we mapped some frontal moraines as well as scattered glacial deposits. These are collectively grouped into three main complexes: Castelletto-Bedoira, Gaiola and Festiona (Fig. 5a,b). Two lateral moraines at different elevations can be linked to these complexes. Moreover, we investigated a frontal moraine well preserved in a lateral hanging valley, Bergemolo (Fig. 6).

CASTELLETTO-BEDOIRA - The lowermost complex of frontal moraines is made up of a series of ridges preserved at an average elevation of about 700 m a.s.l., between the villages of Castelletto and Bedoira (Fig. 5a). We were able to define the ridge of two lateral-frontal moraines preserved on both sides of the valley, although they emerge only 3-5 m from the surrounding surface because they have been partially buried by slope/alluvial deposits and intensely reworked by fluvial actions and agricultural activities. The smoothed ridges show a fairly curved geometry, and their convergence towards the valley centre enabled us to infer two frontal moraine arches. A third lateral-frontal moraine was found on the right side of the valley, near the village of Bedoira (Fig. 5a). It consists of an arch-shaped ridge whose ideal geometric continuation converges towards the valley centre a little farther downstream than the previous described moraines.

The deposits of all these moraines are made up of chaotic accumulations of heterometric boulders and cobbles, predominantly made up of crystalline lithotypes, frequently coated by a clayey reddish film, and in some cases exhibiting slight ferruginous encrustations. Even the sporadic limestone blocks clearly denote a severe state of alteration which led to the formation of numerous dissolution cavities. The matrix, relatively abundant in the first 50-60 cm of depth, is predominantly silty-clay, and shows a very intense reddish colour.

We sampled three large boulders standing on the surface of the more external latero-frontal moraine, a little bit upslope the village of Bedoira (Bedoira samples; Fig. 3a-c).

GAIOLA – A second group of frontal moraines is evident at an average elevation of about 720 m a.s.l., near the village of Gaiola (Fig. 5a), ~2.5 km upvalley the Castelletto-Bedoira moraines. We reconstructed a very distinct frontal ridge and a series of smoothed surface undulations which, due to the shape and composition of the deposits, we consider representative of the top part of moraine ridges emerging from younger surrounding alluvial deposits. The most evident ridge is located in the western sectors of the alluvial plain and extends up to a maximum elevation of about 727 m a.s.l. Two less evident lateral-frontal ridges are present slightly farther downstream; their crests rise only 3-5 m above the alluvial plain (Fig. 5a).

The deposits of this complex are very washed out, evidenced by the cobbles and heterometric boulders often showing a clast-supported structure. The scarce matrix is mainly silty-sand with local clay. The boulders and cobbles are mainly made up of crystalline lithotypes and less frequently of carbonate rock types. Evidence of alteration of the boulders/cobbles is scarce and only those with calcareous composition show the presence of some dissolution cavities. No boulder/pebble is rubefacted. In general, the deposits of this moraine complex show a state of alteration lower than that of the Castelletto-Bedoira complex, but a comparable preservation state of the moraine ridges.

We could not find boulders on the surface of these moraines suitable for sampling.

FESTIONA - This moraine complex consists of three distinct ridges preserved near the village of Festiona (Fig. 5b). The innermost frontal ridges are located at an average elevation of about 730 m a.s.l. and extend towards the current main valley axis. They have an arched shape and a "scissor" arrangement, caused by the partial coalescence of the two ridges. The ridge crests are about 10 meters higher than the alluvial terrace within which they sit and are strongly affected by fluvial erosion. To the SE of these moraines, we found a third moraine ridge, which is partially buried by an alluvial-torrential fan and also dismantled by fluvial processes (Fig. 5b). It corresponds to a small and sharp ridge that, having a slightly arched shape, is elongated transversely with respect to the main valley axis. A few hundred meters to the SW of this moraine, we found another arched-shaped moraine ridge. These two moraines consistently represent the outermost latero-frontal moraine ridge of the Festiona complex (Fig. 5b). Given the altitude (~870 m asl), the glacial deposit partly mantling the rock dorsal south to Demonte does not seem to be connected to the Festiona frontal moraines (~ 760 m asl).

All the moraines of the Festiona complex are characterized by the chaotic accumulation of heterometric blocks and cobbles with a generally sub-angular shape and composed by crystalline lithotypes outcropping upstream of this valley sector. Both blocks and cobbles are generally supported by a predominantly sandy matrix, and do not show any preferential orientation of their axes. The matrix shows a reddish-brown colour in the shallower layers and becomes progressively dark-grey passing to the deeper ones. Overall, the deposits of the Festiona complex show landform evidence comparable with those of the Gaiola and Castelletto-Bedoira complexes but a clearly lower degree of boulders/cobbles weathering alteration.

We sampled five large boulders that stand on the surface of the more external latero-frontal moraine, SW from the village of Festiona (Festiona samples; Fig. 3d-h).

BERGEMOLO - The Bergemolo valley is a hanging valley on the right flank of the main Stura valley (Fig. 1c). Here, we found an internal moraine ridge forming a complete, well-preserved arch with a frontal part at an average elevation of about 1,375 m a.s.l.. Furthermore, we also detected three moraine ridges that collectively draw a single outermost lateral-frontal arch deposited in an earlier and more extensive glacial phase (Fig. 6).

All the moraine deposits are composed of heterometric boulders and cobbles with a prevalent sub-angular shape. The lithological composition is exclusively crystalline, consistent with the bedrock outcropping upvalley. The relatively abundant sandy matrix is brown to grey in colour. The weathering of boulders and cobbles is minimal.

Overall, the internal moraine arch of Bergemolo shows a higher degree of preservation than the other moraine complexes, and limited alteration of the coarse fraction or the matrix. This may be due to less intense post-glacial fluvial erosion relative to the Castelletto-Bedoira moraines.

We sampled three large boulders standing on the surface of the more internal latero-frontal moraine, NW from the Arpione saddle (Bergemolo samples; Fig.4-c).

Glacial modelling

The 3D modelling of the glacier that deposited the Castelletto-Bedoira moraine returned a valley glacier fed by numerous, small tributary glaciers, mostly from the right flank of the main Stura Valley (Fig. 7a). The reconstructed glacier had a surface area of 399 km^2, a volume of 63 km^3 and maximum ice thickness of 622 m. Some large tributary glaciers were present, and these joined the main glacier in the lower-middle sector of the valley both from the left, NE, and the westsides of the basin. The glacial reconstruction matches with the erosive (lateral glacial scarps in the valley flank) and depositional (lateral moraines) evidence found on the ground (Fig. 5a, b). The ELA of the Castelletto-Bedoira glacier was 1,796 m a.s.l..

We did not reconstruct the palaeoshape of the glacier that deposited the Gaiola moraine complex as the modest difference in altitude between, and distance from, the Castelletto-Bedoira moraine would have returned a nearly identical glacier and ELA value.

The reconstructed Stura glacier that deposited the Festiona moraine complex had a surface area of 330 km^2, a volume of 47 km^3, maximum ice thickness of 583 m, and an ELA of 1,802 m a.s.l. (AABR = 1.6). This palaeoglacier was also a valley glacier, fed by the same tributary glaciers entering from the right flank of the Stura Valley as that of Castelletto-Bedoira (Fig. 7b). Preliminary morphological and sedimentological studies suggest that the large left lateral Arma Valley glacier had disconnected from the main Stura glacier at this stage (Capitani, 2002; Spagnolo, 2007), though notice that a reconstruction of the main Stura glacier which includes the contribution from a hypothetical Arma glacier leads to an identical ELA.

The modest palaeoglacier that deposited the Bergemolo frontal moraine resulted from the confluence of four minor glacial tongues (Fig. 8). The glacier had a surface area of 1.5 km^2, a volume of 0.7 km^3 and maximum ice thickness of 88 m. The ELA of the Bergemolo glacier was 1,821 m a.s.l. (AABR = 1.6).

Exposure ages

Our new cosmogenic ^{10}Be boulder exposure ages are presented in Table 1 (Cyr et al., 2022). In the following section, stated uncertainties on individual boulder ages are the analytical uncertainty, followed by the external uncertainty (in parentheses), which considers uncertainties in ^{10}Be production rate and scaling. The analytical uncertainty should be used when comparing our new ^{10}Be exposure ages to one another, whereas the external uncertainty should be used when comparing exposure ages to numeric chronologies determined by other methods and ages from widely separated locations. Ages of the moraines as landforms are calculated as error-weighted means with one- and (two)-standard deviations of the mean, after removing any outliers as identified by the online calculator formerly known as the CRONUS-Earth online exposure age calculator (Balco et al., 2008). Because we observed no evidence of significant surface erosion on sampled boulders (e.g., dissolution cavities, flakes, high intergranular relief), we consider only the ages determined for a 0 mm/kyr boulder surface erosion rate scenario. These ages are, on average, ~5% younger than boulder ages calculated using a surface erosion rate of 3 mm/kyr. This approach is also consistent with previous work in the upper Stura Valley (Spagnolo and Ribolini, 2019) and in the adjacent Gesso Valley (Federici et al., 2008; Federici et al., 2012; Federici et al., 2017).

Three boulder ages from the Bedoira moraine are between 23.2 ± 1.4 (2.0) ka and 24.5 ± 1.6 (2.2) ka (Table 1; Cyr et al., 2022). Statistical analysis using the online calculator (Balco et al., 2008) did not identify any outliers among the three boulder ages, resulting in a mean age of the moraine of 23.6 ± 0.7 (1.6) ka (Fig. 9, 10).

Five boulders sampled on the Festiona moraine yielded ages ranging from 16.5 ± 2.3 (2.5) ka to 28.2 ± 2.3 (2.8) ka (Table 1; Cyr et al., 2022). The online calculator identified one outlier (Festiona-1) and calculated an error-weighted mean age of the moraine of 18.8 ± 0.4 (1.2) ka (Fig. 9, 10).

Three boulders sampled from the Bergemolo moraine yielded individual ages between 16.8 ± 0.6 (1.2) ka and 25.2 ± 4.5 (4.7) ka (Table 1; Cyr et al., 2022). The online calculator identified one outlier (Bergemolo-1) and calculated an error-weighted mean age of the moraine of 21.8 ± 1.4 (1.9) ka (Fig. 9, 10).

Climate at the ELA

In the temporal interval covered by LGM age range, 22.9- 24.3 ka, which is consistent with the 23.6 ± 1.6 ka or 25.0 ± 1.8 ka mean ages of the outermost moraine at Castelletto-Bedoira, and at the altitude of Lago della Costa (7 m a.s.l.), the chironomid-inferred average T_{July} is 14.1 °C (Samartin et al., 2016). The average T_{July} for the age intervals covered by the other two glacial retreat phases, 18.8 ± 1.2 ka or 19.7 ± 1.3 ka at Festiona, and 21.8 ± 1.9 ka or 23.0 ± 2.1 ka at Bergemolo for 0 or 3 mm/ky boulder surface erosion rate, respectively, are 14 °C and 13.3 °C. These correspond to 2.7 °C, 2.3 °C, and 1.6 °C at the Castelletto-Bedoira, Festiona, and Bergemolo glaciers ELAs, respectively. The corresponding annual palaeoprecipitation values are 1,623 mm/yr, 1,527 mm/yr and 1,339 mm/yr. These results are based on the 0 mm/kyr surface erosion rate scenario.

We calculated the modern annual values of T_{July_m} and P_{ann_m} at the LGM ELA (~1,800 m a.s.l.) using the climatic data available for the meteo-stations of the Stura Valley Capitani, 2002). The climate recordings cover 10 years for T and 30 years for P. We obtained the thermal (0.006 °C/m), pluviometric (0.0445 mm/m) and nivometric (0.35 cm/m) lapse rates by running a linear regression between the corresponding values recorded by meteo-stations at different elevations. We estimated the water equivalents of snow using a snow density of 250 kg/m^3, which is representative of values in the range of snow density associated with settled snow (Muskett, 2012; Venäläinen et al., 2021). The analysis returned a modern annual T_{july} of 6.5 °C at the LGM ELA, with P_{total} of 2,415 mm.

Discussion

Glacial evolution

We use our new exposure ages to establish the timing of the glacial standstills that deposited the moraines found in the middle-lower Stura Valley. 2

Our geochronologic data indicate that the Castelletto-Bedoira moraine complex corresponds to the LGM glacial expansion, and that the glacier started to retreat at ~24 ka (mean boulder age of 23.6 ± 0.7 (1.6) ka). After a standstill that led to the formation of the Gaiola moraine complex, the glacier retreated further prior to a new readvance/standstill at approximately ~19 ka (mean boulder age of 18.8 ± 0.4 (1.2) ka), which resulted in the deposition of the Festiona moraine complex. This age is correlative with the Bühl stadial in the Alpine glacial chronology (Ivy-Ochs et al., 2008; Ivy-Ochs, 2015), which occurred during the Oldest Dryas hemispheric cold event. This stadial is locally constrained in the Alps (van Husen 1977; Ivy-Ochs et al., 2018; Braakhekke et al., 2020; Kamleitner et al., 2022), where it is associated with small moraines and marginal deposits produced by a glacial standstill likely caused by a combination of climate forcing and ice-mechanical processes (Reitner 2005).
Our surface exposure ages demonstrate that the glacial readvance that formed the Bergemolo moraine occurred in the time interval between those of Castelletto-Bedoira and Festiona, at approximately 22 ka (mean boulder age of 21.8 ± 1.4 (1.9) ka), most likely at the time of deposition of the moraine complex of Gaiola. The Bergemolo and, likely, the Gaiola moraines therefore represent an early recessional phase that occurred shortly after the LGM climax. Such a reconstruction of glacial evolution requires that the main Stura glacier retreated ~ 7 km in ~4-6 ka from the LGM to the Bühl stadial and that this retreat was interrupted by a short-lived standstill or readvance, capable of forming moraine ridges of Gaiola, while at this point in time the Bergemolo glacier had already separated from the main Stura glacier.

The values of the ELAs for the LGM, including the recessional phase of Bergemolo and Bühl stadials (i.e., the Castelletto-Bedoira and Festiona frontal moraines) are very similar, indicating that the climatic forcing that controlled the glaciers expansions at these times were comparable.

The LGM and early retreat phases in the Maritime Alps

The isotope analyses of the terminal moraines of the Stura (~24 ka, ages between 23.2 ± 1.4 and 24.5 ± 1.6 ka) and the adjacent Gesso (~23 ka, ages between 23.9 ± 0.1 and 21.5 ± 1.0 ka) valleys (Federici et al., 2017) indicate a global LGM exposure age for both. The reconstructed LGM Stura glacier (399 km^2) was about twice as large as the LGM Gesso glacier (204 km^2) (Fig. 11). Despite both terminal moraines being affected by intense post-glacial fluvial erosion, the Stura moraines are much better preserved (both in terms of size and original geometry) than the Gesso counterpart. The reconstructions of the LGM palaeoglaciers in both valleys, carried out with a consistent approach, returned comparable ELA values, 1,796 m a.s.l. and 1,845 m a.s.l. for the Stura and Gesso glaciers, respectively (Federici et al., 2017).

Similar to the Stura Valley, where the Gaiola moraine complex was found near the Castelletto-Bedoira complex, remains of lateral moraines and scattered glacial deposits are evident shortly upvalley from the LGM terminal moraine of the Gesso Valley (i.e., the undated Valdieri-La Bastia deposits) (Federici et al., 2017). Upvalley of these deposits, the first post-LGM Gesso frontal moraine, the Ponte Murato moraine, was constrained to an average exposure age of about ~18.4 ka (ages between 16.9 ± 1.1 and 19.8 ± 0.8) (Federici et al., 2017), which is indistinguishable in exposure age from its counterpart in the Stura Valley, the Festiona moraine complex, which has a mean age of 18.8 ± 0.4 (1.2) ka. The ELA values are also comparable, 1,873 m a.s.l. and 1,802 m a.s.l. for the Murato and Festiona moraines, respectively, and the reduction in length of the corresponding glacial tongue with respect to that of the LGMis ~7 km in both valleys.

In summary, the Maritime Alps (Italian side) recorded their maximum Late Pleistocene glacial expansion in the Global LGM (26-19 ka) (Clark et al., 2009), and consistently with the substadial GS-2.1c recorded in the isotopic chronology of Greenland ice cores (GRIP; Bjork et al., 1998; Loewe et al., 2008; Rasmussen et al., 2014). The first phase of glacial retreat (Bühl Stadial) can be associated to the cold hemispheric event framed between 17.5 and 21 ka (GS-2.1b) (Rasmussen et al. 2014.

A (closer) look at the rest of the Southern Alps

By correlating the exposure ages of terminal moraines/amphitheaters in the Alps (cf. Kamleitner et al. 2022), data obtained for the Maritime Alps complete a picture of synchroneity for the glacial expression of MIS2 across the Southern Alps. This is especially true in its western sector (Fig. 12), where most LGM moraines have comparable cosmogenic nuclide exposure ages: 24.0 ± 1.5 ka in the Susa Valley (Rivoli-Avigliana amphitheater; Ivy-Ochs et al., 2018), 26.5-23.0 ka in the Ossola Valley (Orta end-moraine; Braakhekke et al., 2020), and 25.0 ± 0.9 ka for the Ossola-Ticino valley system (Verbano end-moraine; Kamleitner et al., 2022). In the central and eastern sectors of the Alps, the ages of most LGM moraines are constrained by means of ^{14}C ages which, for the most part, are also consistent with those found in the western sector (Fig. 12).

The compilation of all the chronologic data across the Southern Alps shows an oscillation of the LGM (recession with respect to the maximum glacial advance) recorded by the glaciers of the western sector of the Alps between about 18-21 ka (Fig. 12). The advance/standstill of the Bergemolo Glacier, potentially coeval with the undated moraines of Gaiola and Valdieri-La Bastia, Stura and Gesso valleys respectively, can be added to this list.

Unlike all other sectors of the Southern Alps, the LGM glaciers of the Maritimes Alps did not reach the piedmont plain, debouching into the upper Po plain near the present city of Cuneo (Fig. 11). This difference is most likely due to the fact that the accumulation area of the LGM Stura and Gesso glaciers was considerably smaller compared to that of the larger glacier systems that reached the Po Plain further to the north and east, because of the relatively low altitude of the Maritime Alps catchment area.*Palaeoclimatic inferences*

In the LGM, the Laurentide Ice Sheet (a 2-3 km high topographic obstacle for air mass circulation) and the cooling of the North Atlantic with consequent southern shifting of the sea-ice margin were the elements that had the strongest influence on climate. These environmental conditions caused the Polar Jet Stream to be deflected southward from ~48 °N to about 40 °N and the westerlies to reach the Alps (Florineth and Schlüchter, 1998; Hofer et al, 2012; Merz et al., 2015). Moreover, some numerical simulations suggest that an additional source of moisture could have come from storm tracks across the SW of Europe. In these models, an increase in cyclonic activity in the Gulf of Genoa is considered to be an important source of humidity for the Southern Alps and the Northern Apennines via SW-NE directed storms (Khulemann et al., 2008). The existence of southern moisture advection to the Southern Alps is consistent with numerical simulations of ice flow (Becker et al., 2016) and the climate information retrieved from some Alpine cave speleothems and cryogenic carbonates (Luetscher et al., 2015; Spötl et al., 2021). Accordingly with the chronologies of these palaeoclimatic archives, this southern moisture advection was found to be dominant in the early phase of LGM (26.5-23 ka), promoting a glacial expansion which occurred synchronously across the Southern Alps (Monegato et al., 2017). The re-establishment of the predominance of the westerly circulation, with the simultaneous reduction of the southern moisture supply, caused the downwasting of the LGM glaciers and forced a recessional phase (Fontana et al. 2014; Monegato et al., 2017). However, this recession was not of the same intensity across the Southern Alps, with the glaciers of the central-western sectors withdrawing to a position rather close to that of the moraines of the former maximum LGM limit (Monegato et al, 2017; Kamleitner et al., 2022). This is possibly due to the fact that the mass balance of these glaciers was mostly affected by the westerlies, the intensity of which either did not vary considerably throughout this period or increased as the southern moisture supply decreased. The glaciers of the central and eastern sectors of the Southern Alps instead received less moisture from the westerlies and relied more heavily on the southern supply. When the southern supply reduced, these glaciers experienced more relevant retreats than their western counterparts.

A closer look at regional palaeoclimate

Glacial-climate models based on mass balance that account for ice dynamics and are constrained by geomorphological data (Becket et al., 2016) indicate a best-fit scenario of LGM in the Southern Alps characterized by a ΔT_{ann} = -12 °C and mean annual precipitation of 47% of the current condition.

The data we obtained from P_{ann} at the LGM ELA are consistent with a reduction of 33%. The T_{july} value at the ELA of the LGM Stura glacier cannot be easily converted into a T_{ann} (given the strong seasonality to be expected for LGM), but points to a less dramatic reduction in temperature than that suggested by some models (Allen et al., 2008; Heyman et al., 2013; Becket et al. 2016). The LGM precipitation scenario based on the palaeoglaciological reconstructions in the Maritime Alps on one side confirms that the Southern Alps experienced a lesser reduction in precipitation than the Northern Alps but, on the other side, that such reduction was less pronounced in the southwesterly portion of the Southern Alps relative to other sectors (33% vs 47%). The less marked difference between the Northern and Southern Alps in terms of precipitation is in line with a more recent vision of a more homogenous climate at the LGM (Seguinot et al., 2018).

Conclusions

During the LGM, the Maritime Alps glaciers covered most of the valleys. Overall, the total ice volume was about 90 km^3, with maximum thicknesses exceeding 500 m. It was therefore an important mountain glaciation in the southern latitudes in which it took place (about 44°N). However, unlike all other Southern Alps LGM glaciers, the Maritime Alps glaciers did not reach the Po piedmont plain.

In addition to tracing the maximum extent of the LGM, we reconstructed the positions of the early retreat phases by mapping the corresponding frontal moraines. Our new exposure ages allowed us to reconstruct the timing of the halts which interrupted the post-LGM withdrawal, which started at about 23.6 ± 0.7 (1.6) ka. We mapped and dated the frontal moraines of a first glacial standstill/readvance, which occurred 21.8 ± 1.4 (1.9) ka at a short distance (~7 km) from the maximum external limit of the LGM, and a second one at 18.8 ± 0.4 (1.2) ka. This morpho-chronological succession is congruent with that obtained in the adjacent Gesso Valley, demonstrating a consistent glacial response to palaeoclimatic forcing, also confirmed by the similarity of the ELA values.

The geomorphologic and chronologic data presented herein permit the comparisons with the rest of the Alps, especially the Southern Alps. The comparison highlights a substantial synchronicity across the Southern Alps both for the phase of maximum advances registered during the LGM, and also for the early retreat phases in the central western sectors. The Maritime Alps experienced a recessional phase in which the glacial tongue retreated slightly from the maximum external limit reached during the LGM climax. This glacial behaviour is similar to that recorded by glaciers in the western sector of the Southern Alps, highlighting how the glaciers' mass balance of this recessional phase was similar to that of the LGM climax glaciers. However, this recessional phase was much more pronounced farther east. This difference between the amount of glacial recession in the different alpine sectors could be explained by the complex relationship, including timing of climatic dominance and geographical area of influence, between the moisture supplied by southern currents sourced in the Gulf of Genoa in the Western Mediterranean, and the moisture advected by the westerlies sourced in the North Atlantic. In the southwestern sector of the Southern Alps, it is possible that the post LGM climax reduction/interruption of the southern current moisture supply, which caused significant downwasting of the LGM glaciers in the central-eastern sectors, was less significant farther to the north and east because of the dominance of the westerlies. Estimates of palaeoprecipitation at the ELA of the LGM and early deglaciation Stura glacier support the hypothesis that the Maritime Alps were wetter than the central-eastern sectors of the Southern Alps at the same times.

More data on LGM glaciers and early retreat phases from sectors of the Alps further north are needed to improve the wider late Pleistocene MIS 2 glacial and palaeoclimatic picture of the Western Alps, with particular attention to the behaviour of other minor or marginal glaciers that might have responded more dynamically to climatic variability. To further explore the contribution of southern advection it will be more insightful to include/improve the chronology of the moraines of the Apennine glaciers, where several terrestrial environmental proxies have demonstrated the crucial influence of the moisture supply from southern currents, some of which were sourced all the way from North Africa, on the LGM glacial expansion (Giraudi, 2017; Baroni et al., 2018; Ribolini et al., 2022). Finally, an improved understanding of how the southward shift of the Polar Jet Stream (Polar Front) influenced the precipitation at the ELA of the Southern Alps LGM glaciers could provide a more complete palaeoclimatic reconstruction.

In this context, the Maritime Alps play a strategic role in disentangling the various components of the atmospheric climate picture during the LGM and Lateglacial, because their geographical position makes them extremely sensitive to the circulation of humid air masses sourced from areas to both the west and north. Given their proximity to the Mediterranean Sea and low latitude, the Maritime Alps also represent a bridge between the terrestrial climate proxies classically used in Alpine palaeoenvironmental reconstructions and the terrestrial/marine ones of reference for palaeoenvironmental reconstructions at more "Mediterranean" latitudes, such as Apennine lake sediments and cave deposits, marine sedimentary bio-records, alkenone-based sea-surface temperature, and phases of loess deposition.

Acknowledgments: The fund “The termination I. The environmental and palaeoclimatic variations occurred during the 25–11 ka period” (leader A. Ribolini) supported this work (Progetti di Ricerca di Ateneo PRA, 2020–21, University of Pisa). Exposure dating was completed with the support of the National Science Foundation, Continental Dynamics Program grant EAR-0208169 (RETREAT) and by PRIME Lab, Purdue University, West Lafayette, IN, USA. We thank Cal Ruleman and Will Odom for thorough and constructive reviews. Any use of trade, firm, or product names is for descriptive purposes only and does not imply endorsement by the U.S. Government.

References

Alessio, M., Allegri, L., Bella, F., Belluomini, G., Calderoni, G., Cortesi, C., Improta, S., Manfra, L., Orombelli, G., 1978. I depositi lacustri di Rovagnate, di Pontida e di Pianico in Lombardia: datazione 14C. Geografia Fisica e Dinamica Quaternaria 1, 131-137

Allen, R., Siegert, M. J., and Payne, A. J., 2008. Reconstructing glacierbased climates of LGM Europe and Russia – Part 2: A dataset of LGM precipitation/temperature relations derived from degreeday modelling of palaeo glaciers Climate of the Past, 4, 249–263, doi:10.5194/cp-4-249-2008.

Balco, G., Stone, J.O., Lifton, N.A., Dunai, T.J., 2008. A complete and easily accessible means of calculating surface exposure ages or erosion rates from ^{10}Be and ^{26}Al measurements: Quaternary Geochronology, v. 3, n. 3, p. 174-195, doi: 10.1016/j.quageo.2007.12.001.

Baroni, C., Guidobaldi, G., Salvatore, M.C., Christl, M., Ivy-Ochs S., 2018. Last Glacial Maximum Glaciers in the Northern Apennines Reflect Primarily the Influence of Southerly Storm-Tracks in the Western Mediterranean. Quaternary Science Reviews, 197, 352–367.

Becker, P., Seguinot, J., Jouvet, G., Funk, M., 2016. Last Glacial Maximum precipitation pattern in the Alps inferred from glacier modelling. Geographica Helvetica 71, 173–187.

Benn, D. I., Hulton, N. R. J. 2010. An Excel (TM) spreadsheet program for reconstructing the surface profile of former mountain glaciers and ice caps. Computers and Geosciences, 36, 605–610.Bernoulli, D., Ambrosi, C., Scapozza, C., Stockar, R., Schenker, F.L., Gaggero, L., Antognini, M., Bronzini, S., 2018. Foglio 1373 Mendrisio (parte Est) con parte Ovest del foglio Como. Atlante geologico della Svizzera, 1:25 000, Note esplicative 152. Bundesamt für Landestopografie swisstopo, Wabern.

Bini, A., 1997. Stratigraphy, chronology and paleogeography of Quaternary deposits of the area between the Ticino and Olona rivers (Italy-Switzerland). Geologia Insubrica 2, 21-46.

Bini, A., Zuccoli, L., Bussolini, C., Corbari, D., Da Rold, O., Ferliga, C., Rossi, S., Viviani, C. ,2004: Glacial history of the southern side of the central Alps, Italy. Developments in Quaternary Sciences 2, 195-200.

Bini, A., Buoncristiani, J., Couterrand, S., Ellwanger, D., Felber, M., Florineth, D., Graf, H., Keller, O., Kelly, M., Schlüchter, C. & Schoeneich, P. 2009: Die Schweiz während des letzteiszeitlichen Maximums (LGM). Bundesamt für Landestopografie swisstopo.

Bini, A., Bussolini, C., Turri, S. & Zuccoli L. 2014: Carta geologica alla scala 1:100.000 dell’anfiteatro morenico del Verbano. Sibrium 28, 24-81.

Björck, S., Walker, M. J. C., Cwynar, L. C., Jhonsen, S., Knudsen, K.-L., Lowe, J. J., Wohlfart, B. & INTIMATE MEMBERS 1998. An event stratigraphy for the Last Termination in the North Atlantic region based on the Greenland ice-core record: a proposal by the INTIMATE group. Journal of Quaternary Science, 13, 283–292.

Bonetto, S., Facello, A., Umili, G., 2017. A new application of curvatool semi-automatic approach to qualitatively detect geological lineaments. Environmental and Engineering Geoscience, 23 (3), 179-190. doi: 10.2113/gseegeosci.23.3.179

Braakhekke, J., Ivy-Ochs, S., Monegato, G., Gianotti, F., Martin, S., Casale, S., Christl, M., 2020. Timing and flow pattern of the Orta glacier (European Alps) during the last glacial maximum. Boreas 49, 315-332.

Brochers, B., Marrero, S., Ballco, G., Caffee, M., Goehring, B., Lifton, N., Nishiizumi, K., Phillips, F., Schaefer, J., and Stone, J., 2016. Geological calibration of spallation production rates in the CRINUS-Earth project. Quaternary Geochronology 31, 188-198.

Capitani, M., 2002. Evoluzione geomorfologica recente della Media e Bassa Valle Stura (Alpi Marittime). Undergraduate dissertation, Facoltà di Scienze Matematiche Fisiche e Naturali, University of Pisa, 225 pp.

Capitani M., Marrucci M., 2008. The demonte terrace in the Stura valley (Maritime Alps) between climatic changes and tectonic movements. Geografia Fisica e Dinamica Quaternaria, 31, 1,5-12.

Carton, A., Bondesan, A., Fontana, A., Meneghel, M., Miola, A., Mozzi, P., Primon, S., Surian, N., 2009. Geomorphological evolution and sediment transfer in the Piave river system (northeastern Italy) since the last glacial maximum. Geomorphologie: Relief, Processus et Environnement, 15, 155-174.

Castelletti, L., Livio, F., Martinelli, E., Michetti, A.M., Motella De Carlo, S., 2013. Recenti ricerche paleoecologiche in ambito lariano svolte in collaborazione fra Università dell'Insubria e Laboratorio di archeobiologia dei Musei Civici di Como. Rivista archeologia dell’antica Provincia e Diocesi di Como, 195, 115-128.

Castiglioni, B., 1940- L’Italia nell’età quaternaria. Carta alla scala 1:200000. Atlante Fisico-Economico d’Italia, TCI, Milano.

Cheng, H., Zhang, H., Sp€otl, C., Baker, J., Sinha, A., Li, H., Bartolome, M., Moreno, A., Kathayat, G., Zhao, J., Dong, X., Li, Y., Ning, Y., Jia, X., Zong, B., Brahim, Y.A., Perez-Mejias, C., Cai, Y., Novello, V.F., Cruz, F.W., Severinghaus, J.P., An, Z., Edwards, R.L., 2020. Timing and structure of the Younger Dryas event and its underlying climate dynamics. Proceeding Natural Academy Science, U.S.A., 117, 23408-23417.Clark et al. 2009.

Clark, P.U., Dyke, A.S., Shakun, J.D., Carlson, A.E., Clark, J., 2009. The Last Glacial Maximum. Science 325, 710–714. https://doi.org/10.1126/science.1172873.Cyr, A.J., Ribolini, A., and Spagnolo, M., 2022. Data release for cosmogenic beryllium-10 exposure ages of moraine boulders in the Stura Valley, Maritime Alps, northwestern Italy. U.S. Geological Survey data release. https://doi.org/10.5066/P9HCE4EC.

Dainelli, G. 1939. Atlante Fisico Economico d'Italia. Consociazione Turistica Italiana (ed), Novara,

Dunne, J., Elmore, D., and Muzikar, P., 1999. Scaling factors for the rates of production of cosmogenic nuclides for geometric shielding and attenuation at depth on sloped surfaces. Geomorphology 27, 3-11.

Durand, Y., Laternser, M., Giraud, G., Etchevers, P., Lesaffre, B., Merindol, L., 2009. Reanalysis of 44 yr of climate in the French Alps (1958–2002): methodology, model validation, climatology, and trends for air temperature and precipitation. J. Appl. Meteorol. Climatol. 48, 429–449.

Ehlers J., Gibbard P. L. (2004). Quaternary glaciations-extent and chronology: part I: Europe. Elsevier, Amsterdam, Netherlands.

Ehlers, J., Gibbard, P.L., Hughes, P.D., 2011. Quaternary Glaciations - Extent and Chronology. A Closer Look. Elsevier, Amsterdam.

Federici, P. R., Granger, D. E., Pappalardo, M., Ribolini, A., Spagnolo, M. & Cyr, A. J. 2008. Exposure age dating and equilibrium line altitude reconstruction of an Egesen moraine in the Maritime Alps, Italy. Boreas, 37, 245–253.

Federici, P. R., Granger, D. E., Ribolini, A., Spagnolo, M., Pappalardo, M. & Cyr, A. J. 2012. Last glacial maximum and the Gschnitz stadial in the Maritime Alps according to 10Be cosmogenic dating. Boreas, 41, 277–291, https://doi.org/0.1111/j.1502-3885.2011.00233.x

Federici P. R., 2012: Introduzione alla morfologia glaciale della Valle Stura di Demonte (Alpi Marittime). In: Memorie della Accademia delle Scienze di Torino. 1. Classe di scienze fisiche, matematiche e naturali, 36

Federici, P.R., Ribolini, A., Spagnolo, M., 2017. Glacial history of the maritime Alps from the last glacial maximum to the little ice age. Geol. Soc. Spec. Publ. 433, 137-159.

Florineth, D., Schlüchter, C., 2000. Alpine evidence for atmospheric circulation patterns in Europe during the last glacial maximum. Quaternary Research, 54, 295-308.

Fontana, A., Monegato, G., Zavagno, E., Devoto, S., Burla, I., Cucchi, F., 2014a. Evolution of an Alpine fluvioglacial system at the LGM decay: the Cormor megafan (NE Italy). Geomorphology 204, 136-153.

Forno M.G., Gianotti F., Racca G., 2010. Palaeoclimatic interpretation of the relations between the main and the tributary glaciers in the lower Dora Baltea Valley. Alpine and Mediterranean Quaternary, 23, 1, 105-124

Furbish, D.J., Andrews, J.T., 1984. The use of hypsometry to indicate long term stability and response of valley glaciers to changes in mass transfer. J. Glaciol. 30, 199–211.

Geologische Bundesanstalt, 2013. Der Alpenraum zum Höhepunkt der letzten Eiszeit. Vienna (Geol. Survey of Austria), https://opac.geologie.ac.at/ais312/dokumente/Poster_Alpenraum%20Eiszeit_opt.pdf

Gianotti, F., Forno, M. G., Ivy-Ochs, S. & Kubik, P. W. 2008: New chronological and stratigraphical data on the Ivrea amphitheatre (Piedmont, NW Italy). Quaternary International 190, 123-135.

Giraudi, C., 2017. Climate evolution and forcing during the last 40 ka from the oscillations in Apennine glaciers and high mountain lakes, Italy. Journal of Quaternary Sciences 32, 1085–1098.

Heiri, O., Koinig, K.A., Spötl, C., Barrett, S., Brauer, A., Drescher-Schneider, R., Gaar, D., Ivy-Ochs, S. , Kerschner, H. , Luetscher, M., Moran, A., Nicolussi, K., Preusser, F., Schmidt, R., Schoeneich, P., Schwörer, C. , Sprafke, T., Terhorst, B., Tinner, W., 2014. Palaeoclimate records 60–8 ka in the Austrian and Swiss Alps and their forelands. Quaternary Science Reviews, 106,186-205. doi.org/10.1016/j.quascirev.2014.05.021.Heyman, B. M., Heyman, J., Fickert, T., and Harbor, J. M., 2013. Paleoclimate of the central European uplands during the last glacial maximum based on glacier mass-balance modeling, Quaternary Research, 79, 49–54.

Hofer, D., Raible, C. C., Dehnert, A., Kuhlemann, J., 2012. The impact of different glacial boundary conditions on atmospheric dynamics and precipitation in the North Atlantic region, Climate of the Past, 8, 935–949, doi:10.5194/cp-8-935-2012

Hughes, P. D. & Gibbard, P. L. 2015. A stratigraphical basis for the Last Glacial Maximum (LGM). Quaternary International, 383, 174–185, https://doi.org/ 10.1016/j.quaint.2014.06.006

Hughes, P.D., Gibbard, P.L., Ehlers, J., 2013. Timing of glaciation during the last glacial cycle: evaluating the concept of a global 'Last Glacial Maximum' (LGM). Earth Sci. Rev. 125, 171–198.

Isotta, F.A., Frei, C., Weilguni, V., Perčec Tadić, M., Lassegues, P., Rudolf, B., Pavan, V., Cacciamani, C., Antolini, G., Ratto, S.M., Munari, M., Micheletti, S., Bonati, V., Lussana, C., Ronchi, C., Panettieri, E., Marigo, G., Vertačnik, G., 2014. The climate of daily precipitation in the Alps: development and analysis of a high-resolution grid dataset from pan-Alpine rain-gauge data. Int. J. Climatol. 34, 1657–1675.

Ivy-Ochs, S., Kerschner, H., Reuther, A., Maisch, M., Sailer, R., Schaefer, J., Kubik, P.W., Synal, H., and Schlüchter, C., 2006, The timing of glacier advances in the northern European Alps based on surface exposure dating with cosmogenic 10Be, 26Al, 36Cl, and 21Ne, in Siame, L.L., Bourlès, D.L., and Brown, E.T., eds., In Situ–Produced Cosmogenic Nuclides and Quantification of Geological Processes: Geological Society of America Special Paper 415, p. 43–60, doi: 10.1130/2006.2415(04).

Ivy-Ochs, S., Kerschner, H., Reuther, A., Preusser, F., Heine, K., Maisch, M., Kubik, P. W. & Schlüchter, C. 2008: Chronology of the last glacial cycle in the European Alps. Journal of Quaternary Science 23, 559-573.

Ivy-Ochs, S. 2015: Glacier variations in the European Alps at the end of the last glaciation. Cuadernos de investigación geográfica 41, 295-315.

Ivy-Ochs, S., Lucchesi, S., Baggio, P., Fioraso, G., Gianotti, F., Monegato, G., Graf, A. A., Akçar, N., Christl, M., Carraro, F., Forno, M. G. & Schlüchter, C. 2018: New geomorphological and chronological constraints for glacial deposits in the Rivoli-Avigliana end-moraine system and the lower Susa Valley (Western Alps, NW Italy). Journal of Quaternary Sciences 33, 550–562.

Kamleitner S., Ivy-Ochs S., Monegato G., Gianotti F., Akçar N., Vockenhuber C., Christl M., Synal H.-A., 2022. The Ticino-Toce glacier system (Swiss-Italian Alps) in the framework of the Alpine Last Glacial Maximum. Quaternary Science Reviews, 279, DOI: 10.1016/j.quascirev.2022.107400

Kelly, M. A., Buoncristiani, J.-F. & Schlüchter, C. 2004: A reconstruction of the last glacial maximum (LGM) ice-surface geometry in the western Swiss Alps and contiguous Alpine regions in Italy and France. Eclogae Geologicae Helvetiae 97, 57-75.

Kohl, C.P., and Nishiizumi, K., 1992. Chemical isolation of quartz for measurement of *in-situ*-produced cosmogenic nuclides. Geochimica et Cosmochimica Acta 56, 3583-3587.

Kuhlemann, J., Rohling, E.J., Krumrei, I., Kubik, P., Ivy-Ochs, S., Kucera, M., 2008. Regional synthesis of mediterranean atmospheric circulation during the last glacial maximum. Science 321, 1338-1340.

Lifton, N., Sato, T., and Dunai, T.J., 2014, Scaling in situ cosmogenic nuclide production rates using analytical approximations to atmospheric cosmic-ray fluxes: Earth and Planetary Science Letters, v. 386, p. 149-160.

Lotter, A.F., Heiri ,O., Brooks, S., van Leeuwen, J.F.N., Eicher, U., Ammann, B. 2012. Rapid summer temperature changes during Termination 1a: high-resolution multi-proxy climate reconstructions from Gerzensee (Switzerland).Quaternary Science Reviews, 36, 103-11. https://doi.org/10.1016/j.quascirev.2010.06.022

Lowe, J.J., Rasmussen, S.O., Bjorck, S., Hoek, W.Z., Steffensen, J.P., Walker, M.J.C., Yu, Z.C. and the INTIMATE group, 2008. Integration of ice-core, marine and terrestrial records (INTIMATE): refining the record of the last glacial–interglacial transition. Quaternary Science Reviews, 27: 6–17.
Luetscher, M., Boch, R., Sodemann, H., Spötl, C., Cheng, H., Edwards, R.L., Frisia, S., Hof, F., Müller, W., 2015. North Atlantic storm track changes during the last glacial maximum recorded by Alpine speleothems. Nature Communications 6, 27-32.Malaroda, R.; Carraro, F. 1970. Carta Geologica del Massiccio dell'Argentera alla scala 1:50.000 e note illustrative. Memorie Società Geologica Italiana,1970, 9, 557–663.
Marrucci M., Zeilinger G., Ribolini A., Schwanghart W., 2018. Origin of knickpoints in an alpine context subject to different perturbing factors, stura valley, maritime alps (North-Western Italy). Geosciences, 8 (12), DOI: 10.3390/geosciences8120443
Merz, N., Raible, C. C., and Woollings, T., 2015. North Atlantic eddydriven jet in interglacial and glacial winter climates, Journal of Climate, 28, 3977–3997.
Monegato G., Ravazzi C., Donegana M., Pini R., Calderoni G., Wick L. (2007) - Evidence of a two-fold glacial advance during the last glacial maximum in the Tagliamento end moraine system (eastern Alps). Quaternary Research, 68(2), 284-302. Doi: 10.1016/j.yqres.2007.07.002.
Monegato, G., Scardia, G., Hajdas, I., Rizzini, F., Piccin, A., 2017. The Alpine LGM in the boreal ice-sheets game. Sci. Rep. 7, 1e8.
Muskett, R.R. 2012. Remote Sensing, Model-Derived and Ground Measurements of Snow Water Equivalent and Snow Density in Alaska. International Journal of Geosciences, 3, ID:25005. DOI:10.4236/ijg.2012.35114.
Musumeci, G.; Ribolini, A.; Spagnolo, M. The effect of late Alpine tectonics in the morphology of the Argentera Massif (Western Alps, Italy–France). Quat. Int. 2003, 101, 191–201.
Nishiizumi, K., Imamura, M., Caffee, M.W., Southon, J.R., Finkel, R.C., McAninch, J., 2007, Absolute calibration of 10Be AMS standards: Nuclear Instruments and Methods in Physics Research B, v. 258, p. 403-413, doi: 10.1016/j.nimb.2007.01.297.
Ohmura, A., Boettcher, M., 2018. Climate on the equilibrium line altitudes of glaciers: theoretical background behind Ahlmann's P/T diagram. J. Glaciol. 64, 489–505.
Paterson, W.S.B., 1994. The Physics of Glaciers, third ed. Pergamon/Elsevier, London.
Pellegrini, G. B., Albanese, D., Bertoldi, R. & Surian, N. 2005: La deglaciazione alpina nel Vallone Bellunese, Alpi meridionali orientali. Supplementi Geografia Fisica e Dinamica Quaternaria 7, 271-280
Pellitero, R., Rea, B. R. et al. 2015. A GIS tool for automatic calculation of glacier equilibrium-line altitudes. Computer & Geosciences, 82, 55–62.
Pellitero, R., Rea, B.R., Spagnolo, M., Bakke, J., Ivy-Ochs, S., Frew, C.R., Hughes, P., Ribolini, A., Lukas, S., Renssen, H., 2016. GlaRe, a GIS tool to reconstruct the 3D surface of palaeoglaciers. Comput. Geosci. 94, 77–85.
Penck A., Brückner E. (1901–1909) - Die Alpen im Eiszeitalter. Tauchnitz, Leipzig, Germany, pp. 1199.
Perello, P.; Piana, F. Neogenic thrust and strike—Slip tectonics at the northen boundaty between the Argentera Massif and its metasedimentary cover. Quad. Geodin. Alp. Quat. 1997, 4, 205.
Rasmussen, S. O., Bigler, M., Blockley, S. P., Blunier, T. , Buchardt, S. L., Clausen, H.B., Cvijanovic, I., Jensen, D.-D., Johnsen, S. J., Fischer, H., Gkinis, V., Guillevic, M., Hoek, W.Z., Lowe J. J., Pedro, J. B., Popp, T., Seierstad, I. K., Steffensen, J. P., Svensson, A.M., Vallelonga, P., Vinther, B.M., Walker, M. J.C., Wheatley, J.J., Winstrup, M. 2014. A stratigraphic framework

for abrupt climatic changes during the Last Glacial period based on three synchronized Greenland ice-core records: refining and extending the INTIMATE event stratigraphy. Quaternary Science Reviews, 106, 14-28. https://doi.org/10.1016/j.quascirev.2014.09.007.

Ravazzi, C., Badino, F., Marsetti, D., Patera, G., Reimer, P.J., 2012. Glacial to paraglacial history and forest recovery in the Oglio glacier system (Italian Alps) between 26 and 15 ka cal BP. Quaternary Science Rev.iews 58, 146-161.

Rea, B. R., R. Pellitero, M. Spagnolo, P. Hughes, S. Ivy-Ochs, H. Renssen, A. Ribolini, J. Bakke, S. Lukas, and R. J. Braithwaite. 2020. Atmospheric Circulation Over Europe during the Younger Dryas. Science Advances, 6, 50. doi:10.1126/sciadv.aba4844

Rea, B. R. 2009. Defining modern day area-altitude balance ratios (AABRs) and their use in glacier-climate reconstructions. Quaternary Science Reviews, 28, 237–248.

Reitner, J.M. 2005: Quartärgeologie und Landschaftsentwicklung im Raum Kitzbühel-St. Johann i.T.-Hopfgarten (Nordtirol) vom Riss bis in das Würm-Spätglazial (MIS 6-2). Ph.D. thesis, University of Vienna, 190 pp.

Reitner, J.M. 2007. Glacial dynamics at the beginning of Termination I in the Eastern Alps and their stratigraphic implications. Quaternary International, 164–165, 64-84

Ribolini, A. Relief distribution, morphology and Cenozoic differential uplift in the Argentera Massif (French-Italian Alps). Z. Geomorphol. 2000, 44, 363–378.

Ribolini A., Fabre D., 2006. Permafrost existence in rock glaciers of the Argentera Massif, Maritime Alps, Italy. Permafrost and Periglacial Processes, 17 (1), 49-63. DOI: 10.1002/ppp.548

Ribolini, A.; Spagnolo, M., 2008.Drainage network geometry versus tectonics in the Argentera Massif (French-Italian Alps). Geomorphology, 93, 253–266.

Ribolini, A., Chelli, A., Guglielmin, M., Pappalardo, M., 2007. Relationship between glacier and rock glacier in the Maritime Alps Schiantala Valley, Italy. Quaternary Research, 68, 353–363.

Ribolini, A., Guglielmin, M. et al. 2010. The internal structure of rock glaciers and recently-deglaciated slopes as revealed by geoelectrical tomography: insights on permafrost and recent glacial evolution in the Central and Western Alps (Italy-France). Quaternary Science Reviews, 29, 507–521.

Ribolini, A., Bini, M., Isola, I., Spagnolo, M., Zanchetta, G., Pellitero, R., Mechernich, S., Gromig, R., Dunai, T., Wagner, B., Milevski, I. 2018. An oldest dryas glacier expansion on mount pelister (former Yugoslavian Republic of Macedonia) according to 10Be cosmogenic dating. Journal of the Geological Society, 175, 1, 100-110.

Ribolini A., Spagnolo M., Giraudi C. 2022. The Italian mountains: glacial landforms from the Last Glacial Maximum. In: Palacios, D., Hughes, P., García-Ruiz, J., Nuria, A, European glacial landscapes. Maximum Extent of Glaciation. Amsterdam, Elsevier, 481-486. https://doi.org/10.1016/B978-0-12-823498-3.00022-4

Rolland, Y., Darnault, R., Braucher, R., Bourlès, D., Petit, C., Bouissou, S., & ASTER Team. (2020). Deglaciation history at the Alpine-Mediterranean transition (Argentera-Mercantour, SW Alps) from 10Be dating of moraines and glacially polished bedrock. Earth Surface Processes and Landforms, 45(2), 393-410.

Samartin S., Heiri O., Kaltenrieder P., Kühl N., Tinner W., 2016. Reconstruction of full glacial environments and summer temperatures from Lago della Costa, a refugial site in Northern Italy. Quaternary Science Reviews, 143, 107-119. DOI: 10.1016/j.quascirev.2016.04.005

Seguinot J., Ivy-Ochs S., Jouvet G., Huss M., Funk M., Preusser F. (2018) - Modelling last glacial cycle ice dynamics in the Alps. The Cryosphere, 12(10), 3265-3285. Doi: 10.5194/tc-12-3265-2018

Shilling, D.H., Hollin, J.T., 1981. Numerical reconstructions of valley glaciers and small icecaps. In: Denton, G.H., Hughes, T.J. (Eds.), The Last Great Ice Sheets. Wiley, New York, 207–220.

Spagnolo, M., 2007.Illustrative notes of the Geomorphological Map of the Upper Arma Valley (Stura di Demonte Valley, Maritime Alps). Geografia Fisica Dinamica Quaternaria, 30, 117–125.
Spagnolo M., Ribolini A., 2019. Glacier extent and climate in the Maritime Alps during the Younger Dryas. Palaeogeography, Palaeoclimatology, Palaeoecology, 536, DOI: 10.1016/j.palaeo.2019.109400
Spötl, C., Koltai, G., Jarosch, A.H., Cheng, H., 2021. Increased autumn and winter precipitation during the last glacial maximum in the European Alps. Nat. Commun. 12.
Stefanini, M. C., Ribolini, A. 2003. Dendrogeomorphological investigations of debris-flows occurrence in the Maritime Alps (northwestern Italy). In: Rickermann, D. & Chen, C. (eds) Debris-Flow Hazard Mitigation. Mechanics, Prediction, and Assessment. Millpress, Rotterdam, 231–242.
Tarquini, S., Isola, I., Favalli, M., Mazzarini, F., Bisson, M., Pareschi, M.T., Boschi, E., 2007. TINITALY/01: a new Triangular Irregular Network of Italy, Annals of Geophysics, 50, 407-425.
van Husen, D., 1977. Zur Fazies und Stratigraphie der jungpleistozänen Ablagerungen im Trauntal (mit quartärgeologischer Karte). Jahrbüch der Geologischen Bundesanstalt, 120, 1–130.
van Husen D., 1987. Die Ostalpen und ihr Vorland in der letzten Eiszeit (Würm). Geologische Bundesanstalt, Vienna.
Venäläinen, P., Luojus,K., Lemmetyinen,J., Pulliainen, J., Moisander, M., Takala, M. 2021. Impact of dynamic snow density on GlobSnow snow water equivalent retrieval accuracy. The Cryosphere, 15, 2969–2981. doi.org/10.5194/tc-15-2969-2021
von Blanckenburg, F., Belshaw, N.S., and O'Nions, R.K., 1996, Separation of 9Be and cosmogenic 10Be from environmental materials and SIMS isotope dilution analysis: Chemical Geology, v. 129, p. 93-99, doi: 10.1016.0009-2541(95)00157-3.

Captions to figures

Figure 1 – LGM extent over the Alps determined by a) Ehlers and Gibbard (2004) and b) Geologische Bundesanstalt (2013). The differences in LGM extent of the Maritime Alps are evident. RV: Rivoli-Avigliana glacier; IV: Ivrea glacier; OR: Orta glacier; VB: Verbano glacier; LR: Lario glacier; IS: Iseo glacier; GR: Garda glacier; TG: Tagliamento glacier. c) geographic sketch map of the Maritime Alps with Stura di Demonte and Gesso valleys indicated. Dashed yellow line represents the border between Italy and France. Position of the geomorphological sketch maps of Figs 4a, b and 5 are reported. Basemap from Shuttle Radar Topography Mission (SRTM).

Figure 2 – Dated (exposure age) moraines in the Maritime Alps. Sources: (1) Federici et al. 2017; (2) Federici et al. 2012; (3) Federici et al. 2008; (4) Spagnolo and Ribolini (2019); (5) Rolland et al. 2020; (6) this paper. Basemap from Shuttle Radar Topography Mission (SRTM).

Figure 3 – Boulders sampled on the Bedoira (a, b, c) and Festiona (d, e, f, g, h) moraine complexes.

Figure 4 - Boulders sampled on the Bergemolo moraine.

Figure 5 – a) Moraines and glacial deposits in the lowermost Stura Valley (see Fig. 1c for location), forming the Castelletto-Bedoira and Gaiola moraine complexes; b) Moraines and glacial deposits in the mid Stura Valley (see Fig. 1c for location), forming the Festiona moraine complex. Purple lines correspond to moraine ridges, violet-filled polygons to glacial deposits, purple lines associated to violet-filled rectangles to glacial scarps, green polygons to terraced-alluvial plains, and green curved-lines to alluvial fans. Black boxes indicate village position. Positions and ages of the sampled boulders are reported. Basemap from TINITALY (Tarquini et al., 2007)

Figure 6 – a) Moraines and glacial deposits in the Bergemolo Valley (see Fig. 1c for location); b) close-up of the Bergemolo main arch with the positions and ages of the sampled boulders. Dark blue lines correspond to moraine ridges, light blue-filled polygons to glacial deposits of the Bergemolo Glacier. Purple lines correspond to moraine ridges, violet-filled polygons to glacial deposits of the main Stura Glacier, green polygons to terraced-alluvial plains, and green curved-lines to alluvial fans. Black boxes indicate village position. Basemap from TINITALY (Tarquini et al., 2007).

Figure 7 – a) reconstruction of the LGM (~23.5 ka) palaeoglacier, terminus marked by the Castelletto-Bedoira moraine complex; b) reconstruction of the early retreat phase (~18.5 ka) palaeoglacier, terminus marked by the Festiona moraine complex. Basemap from Shuttle Radar Topography Mission (SRTM).

Figure 8 - Reconstruction of the LGM early retreat phase (~21.5 ka) palaeoglacier, terminus marked by the Bergemolo moraine. Basemap from TINITALY (Tarquini et al., 2007).

Figure 9 - Normal kernel density estimates of individual boulders (dashed gray curves) and moraines (black curves) in Stura Valley using boulder surface erosion rates of 0 mm/kyr (a) and 3 mm/kyr (b). Error-weighted mean ages of moraine deposits, with 2-standard error, are indicated by the vertical dotted gray lines and boxes, respectively. Individual boulder ages identified as outliers by the single landform tool in version 3 of the online calculator formerly known as the CRONUS-Earth online calculator (Balco et al., 2008; http://hess.ess.washington.edu), are shown with the areas under the curves shaded gray.

Figure 10 - Comparison of individual boulder (circles) and moraine (boxes) ^{10}Be exposure ages calculated under zero mm/kyr boulder surface erosion rates from the Bedoira (blue), Festiona (orange), and Bergemolo (green) moraines. Outliers, identified by the single landform tool in version 3 of the online calculator formerly known as the CRONUS-Earth online calculator (Balco et al., 2008; http://hess.ess.washington.edu), are shown with gray outlines and were not included in the determination of the error weighted mean and two standard deviation age range indicated by the colored boxes.

Figure 11 – The LGM glacial scenario in the Maritime Alps (Italian side) around 23.5 ka. The total ice volume consisted of about 90 km^3 (62.9 km^3 and 26.6 km^3 for the Stura and Gesso glaciers, respectively), with

maximum thicknesses exceeding 500 m (620 m and 515 m, respectively). Basemap from Shuttle Radar Topography Mission (SRTM).

Figure 12 – Synoptic scheme of the LGM climax and LGM recession in the Southern Alps and Northern Apennines. Exposure ages in the white boxes, 14C ages in the grey boxes. Sources of the glacial chronology: (1) Federici et al. 2011, 2017; (2) this paper(Cyr et al., 2022); (3) Ivy-Ochs et al., 2018; (4) Giannotti et al., 2008, 2015; (5) Braakhekke et al., 2020; (6) Kamleitner et al., 2022; (7) Castelletti et al.,2013; Bernoulli et al., 2018; (8) Alessio et al., 1978; Bini, 1997; (9) Ravazzi et al., 2012; (10) Monegato et al., 2017; (11) Carton et al., 2009; (12) Monegato et al., 2007; (13) Baroni et al., 2018. Basemap from Shuttle Radar Topography Mission (SRTM).

Figure 1

Click here to access/download;Figure;FIG_1_NEW.jpg

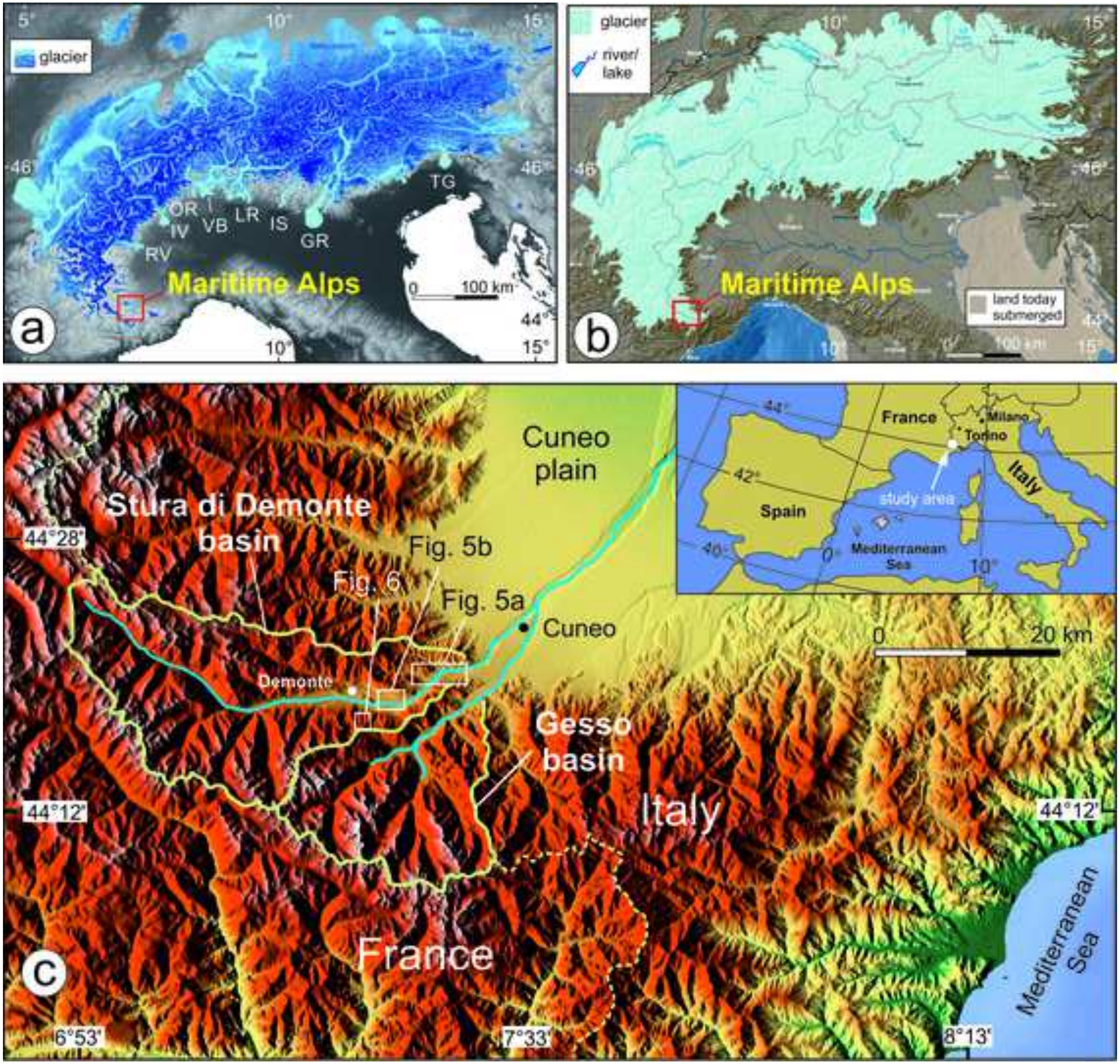

Figure 2

Click here to access/download;Figure;Fig_2 new.jpg

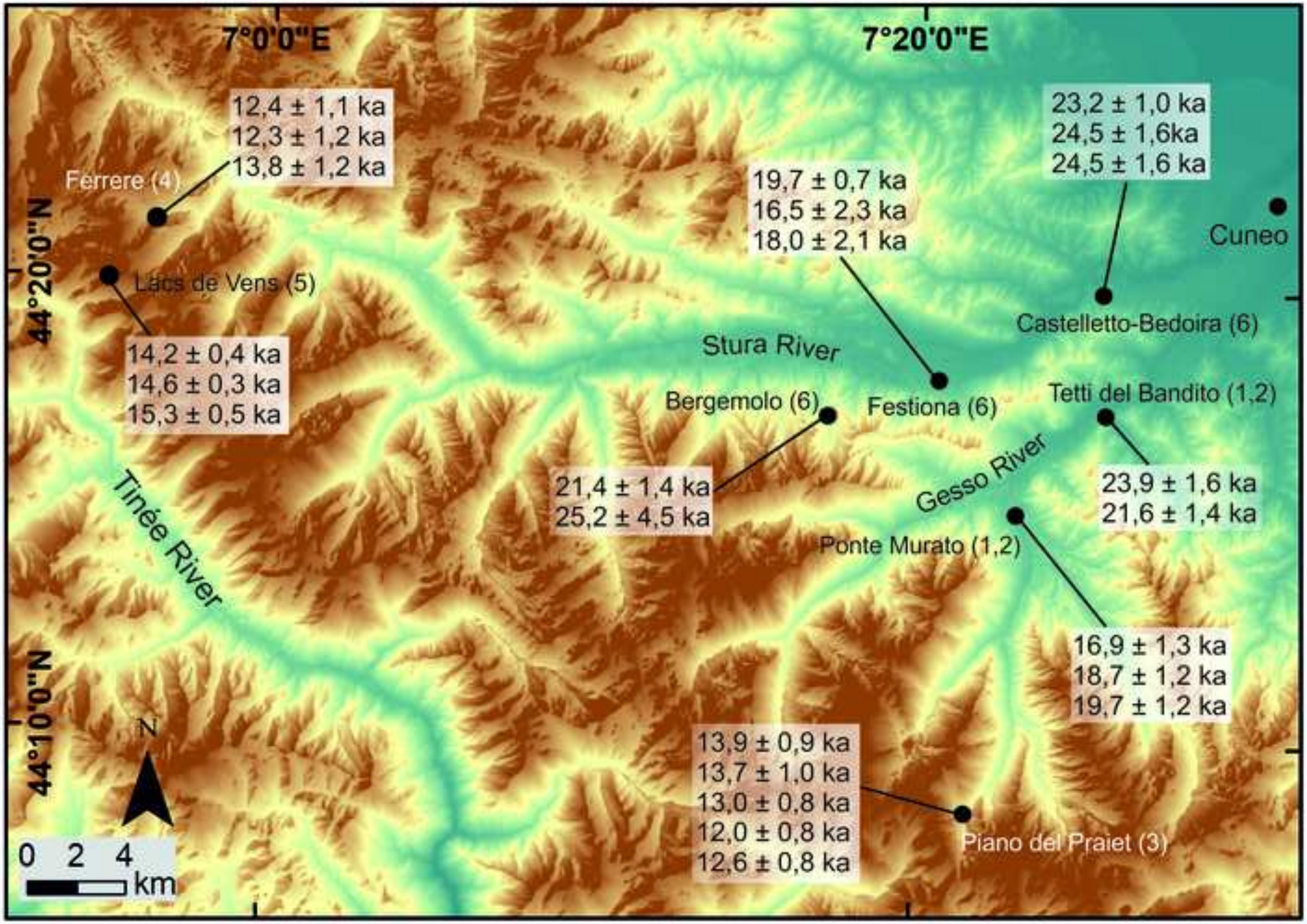

Figure 3

Click here to access/download;Figure;FIG_3.jpg

Figure 4

Figure 5

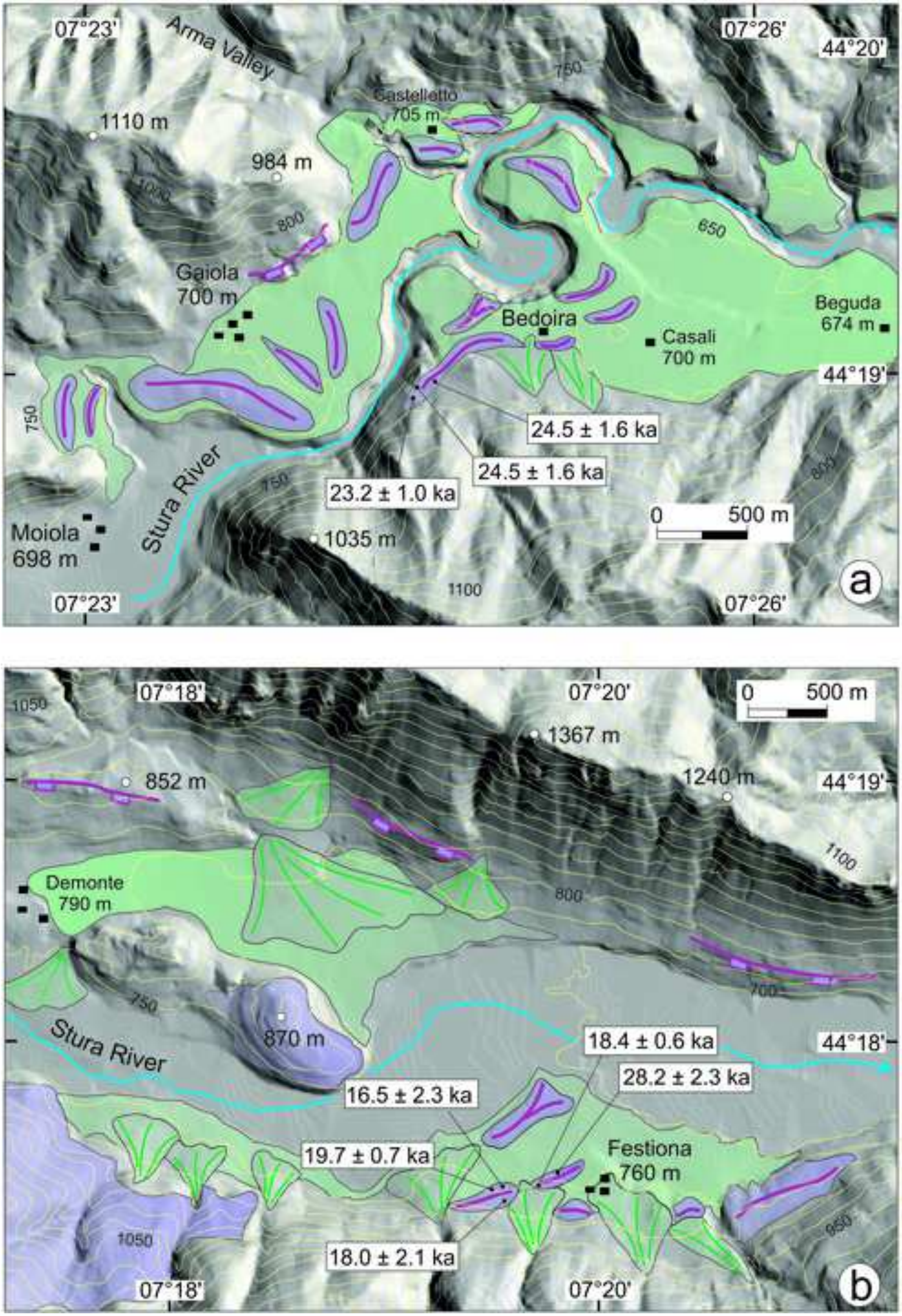
07°23'
Arma Valley
07°26'
44°20'
750
Castelletto
705 m
1110 m
984 m
1000
800
650
Gaiola
700 m
Bedoira
Casali
700 m
Beguda
674 m
44°19'
750
24.5 ± 1.6 ka
24.5 ± 1.6 ka
23.2 ± 1.0 ka
Stura River
750
800
0
500 m
Moiola
698 m
1035 m
1100
07°23'
07°26'
a
1050
07°18'
07°20'
0
500 m
1367 m
852 m
1240 m
44°19'
1100
Demonte
790 m
800
750
700
870 m
Stura River
18.4 ± 0.6 ka
44°18'
28.2 ± 2.3 ka
16.5 ± 2.3 ka
19.7 ± 0.7 ka
Festiona
760 m
950
1050
18.0 ± 2.1 ka
07°18'
07°20'
b

Figure 6

Click here to access/download;Figure;FIG_6_NEW.jpg

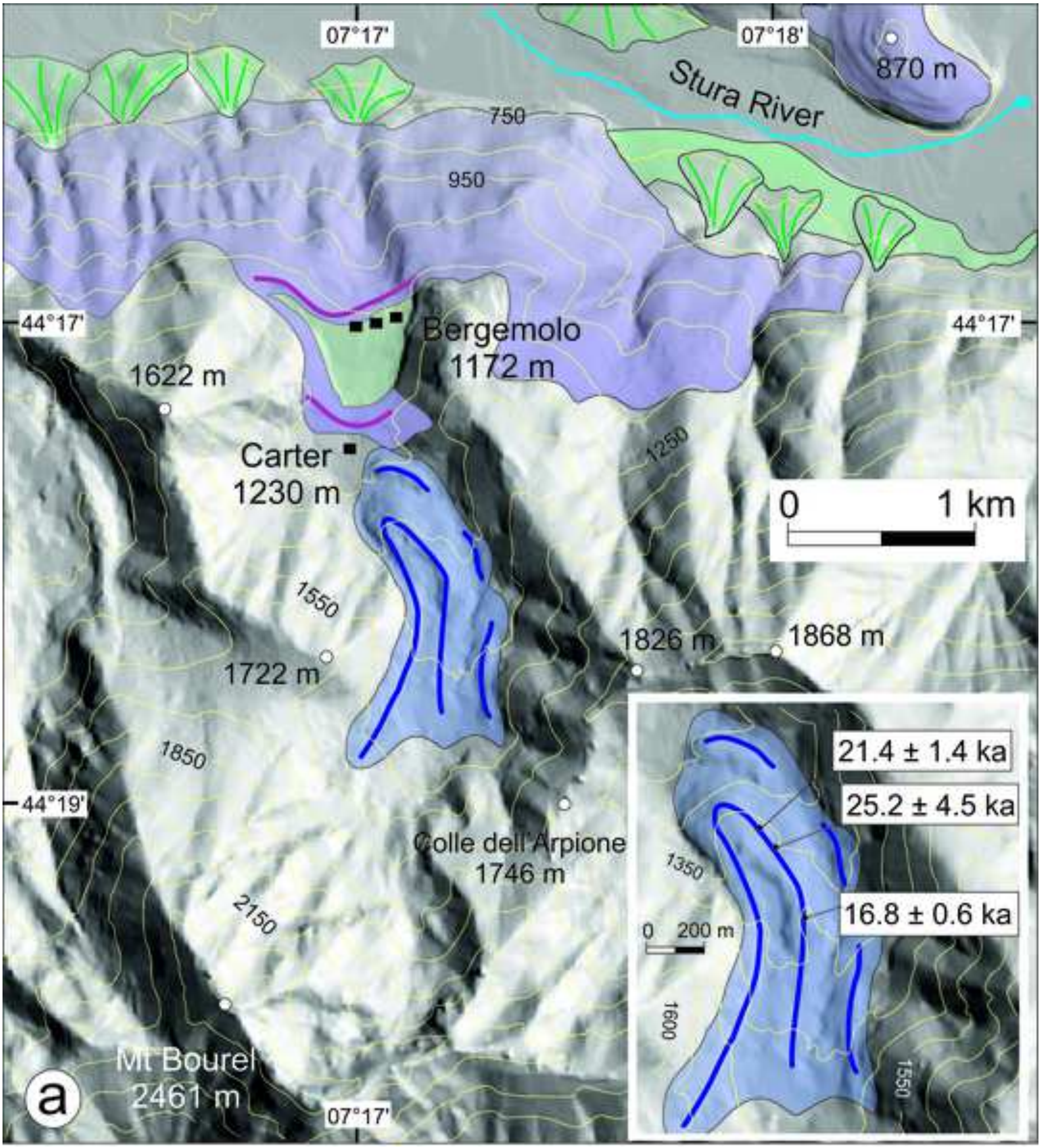

Figure 7

Click here to access/download;Figure;FIG_7new.jpg

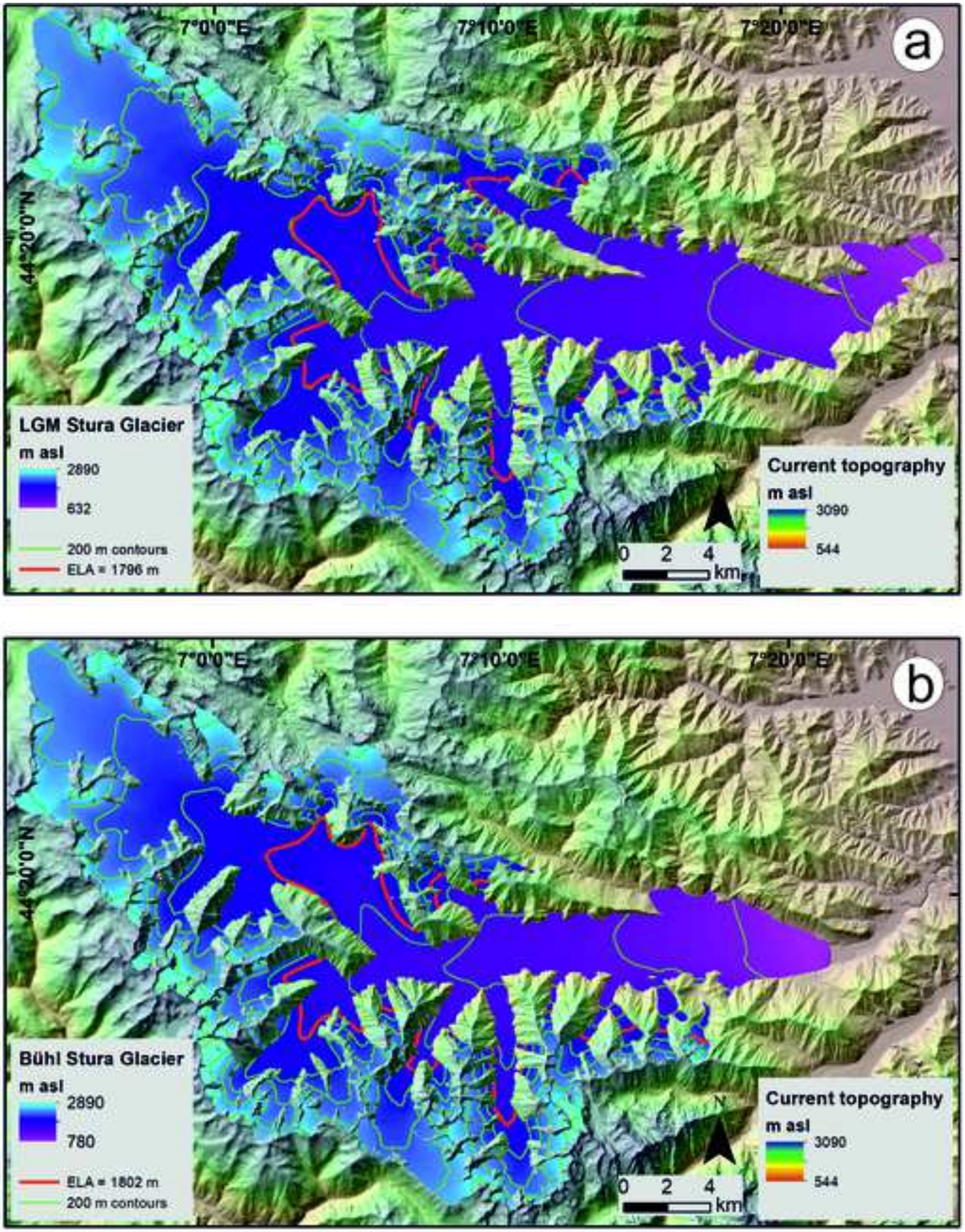

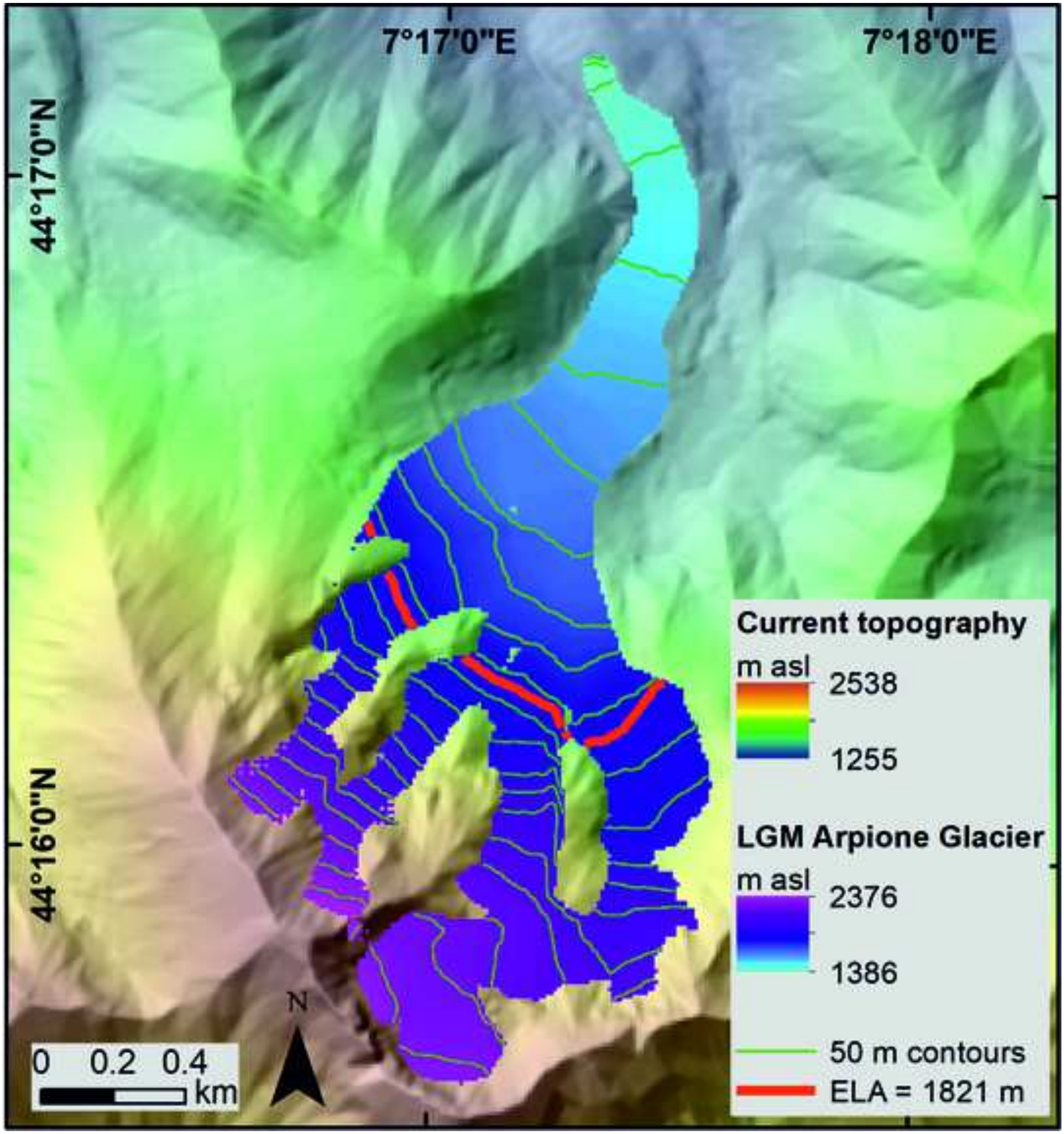
7°17'0"E
7°18'0"E
44°17'0"N
44°16'0"N
Current topography
m asl
2538
1255
LGM Arpione Glacier
m asl
2376
1386
50 m contours
ELA = 1821 m
0 0.2 0.4
km
N

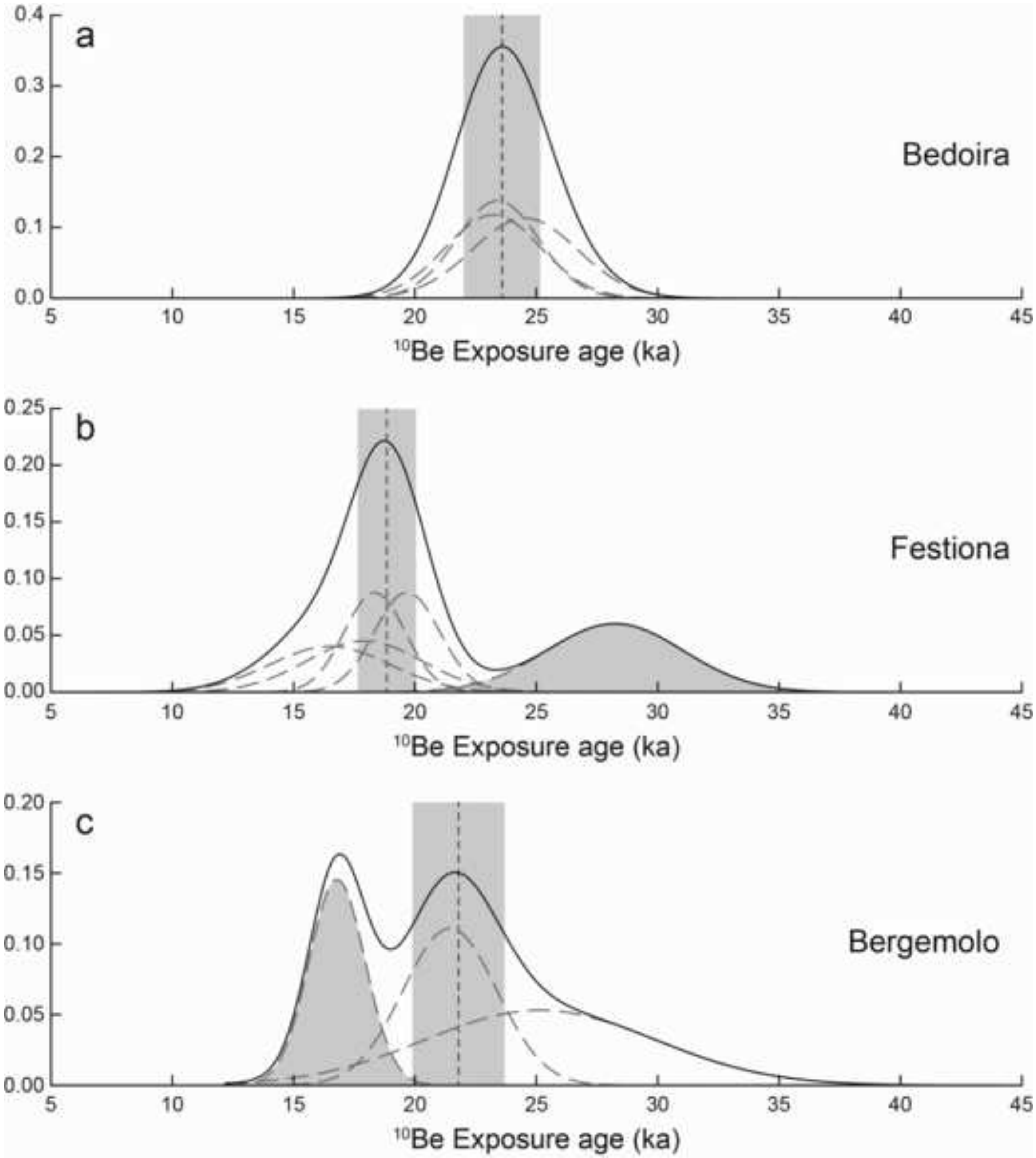

a
Bedoira
0.4
0.3
0.2
0.1
0.0
5
10
15
20
25
30
35
40
45
^{10}Be Exposure age (ka)
b
Festiona
0.25
0.20
0.15
0.10
0.05
0.00
^{10}Be Exposure age (ka)
c
Bergemolo
0.20
0.15
0.10
0.05
0.00
^{10}Be Exposure age (ka)

Figure 10

Click here to access/download;Figure;FIG_10_NEW.jpg

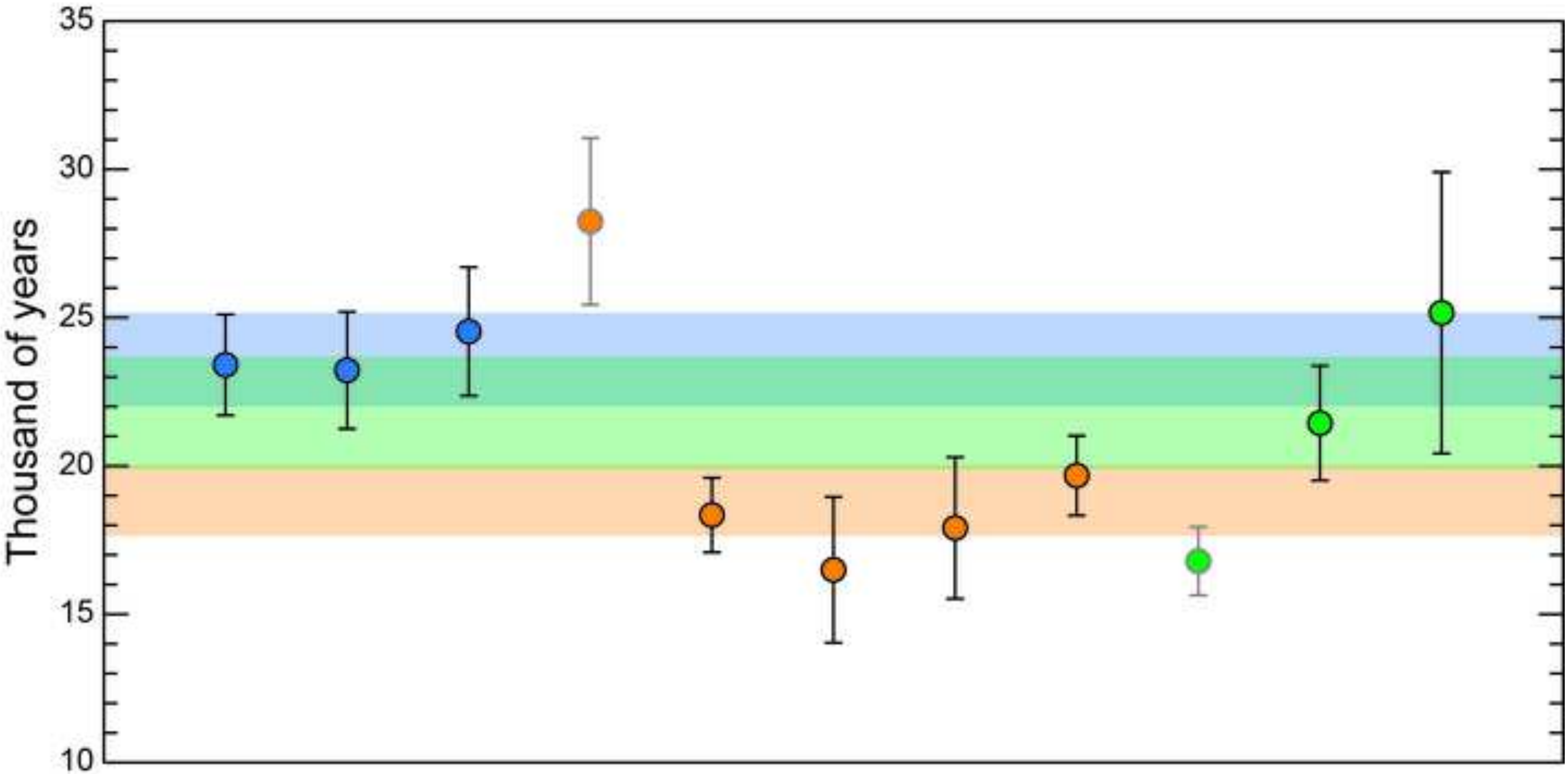

Figure 11

Click here to access/download;Figure;FIG_11_NEW.tif

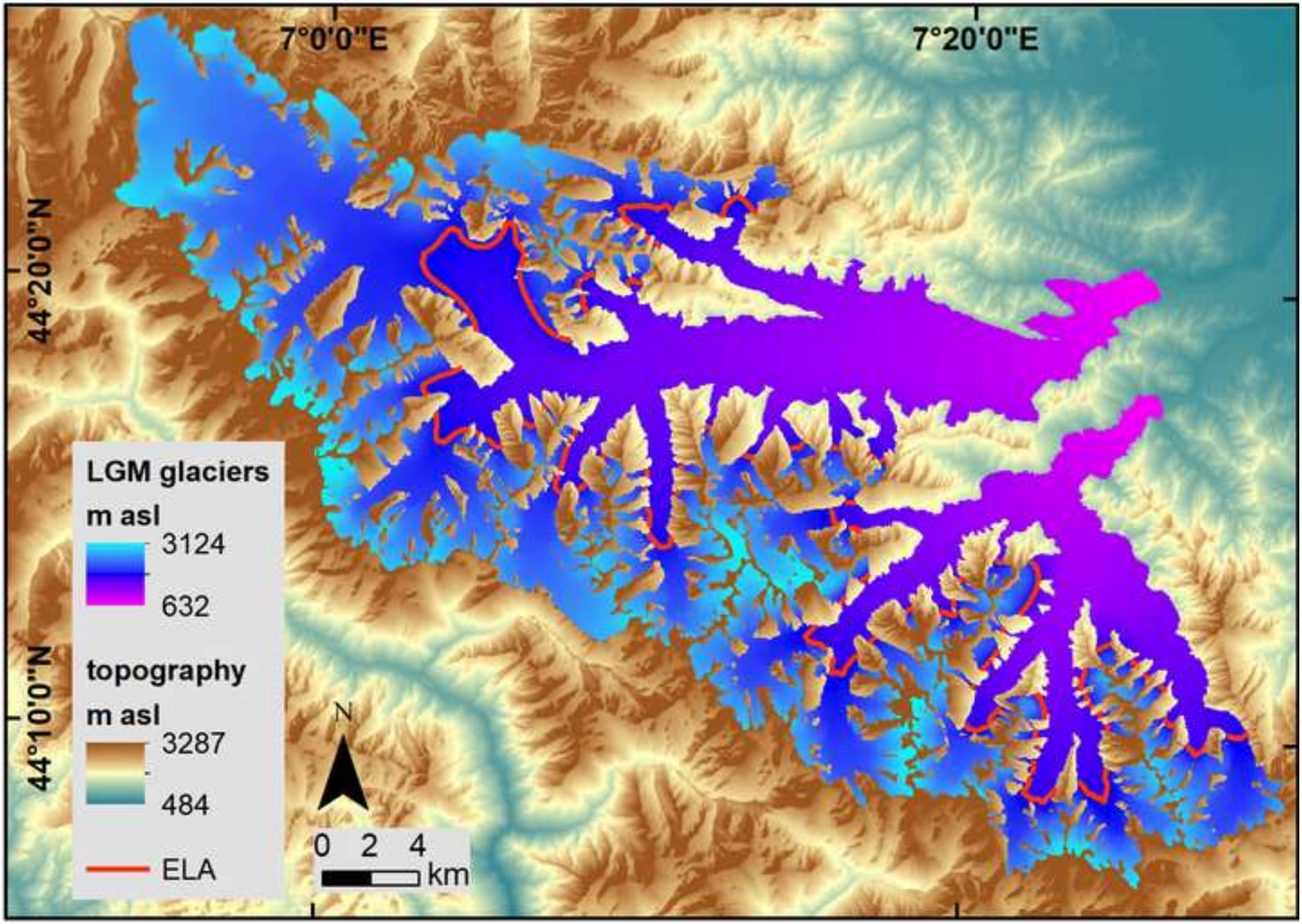

Figure 12

Click here to access/download;Figure;FIG_12.jpg

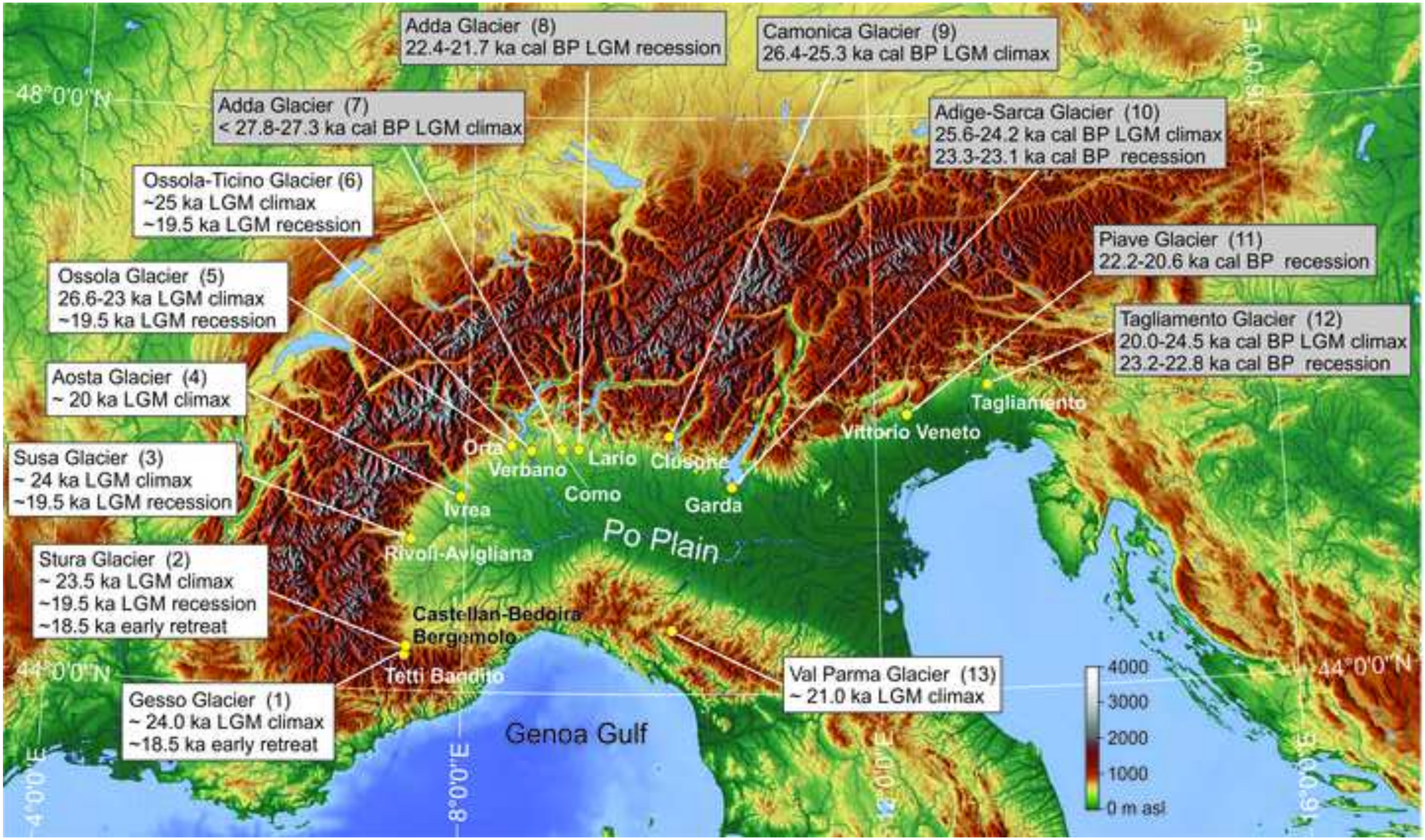

Table 1

Click here to access/download;Table;Table_1_Ribolini_and_others_Stura_corrected.xlsx

TABLE 1. Cosmogenic 10Be sample information and exposure ages of moraine boulders in the Stura Valley, Maritime Alps, Italy.

Sample ID	Latitude[a] (DD WGS84)	Longitude[a] (DD WGS84)	Elevation (m)	Elevation flag	Thickness (cm)	Density ($g\ cm^{-3}$)	Shielding factor[b]	Year collected	Nuclide	Mineral	Nuclide standardization	Nuclide concentration [10Be][c] ($atoms\ g\ quartz^{-1}$)	Nuclide concentration [10Be] uncertainty[c] ($atoms\ g\ quartz^{-1}$)	$0\ mm\ kyr^{-1}$ Exposure age[d] (yr)	$0\ mm\ kyr^{-1}$ Internal uncertainty[e] (yr)	$0\ mm\ kyr^{-1}$ External uncertainty[f] (yr)	$0\ mm\ kyr^{-1}$ Exposure_age[d] (yr)
Bedoira 1	44.3285	7.4169	790	std	3	2.65	0.972	2006	Be-10	quartz	07KNSTD	176,815	7,361	23,407	980	1,700	24,832
Bedoira 2	44.3286	7.4164	760	std	3	2.65	0.972	2006	Be-10	quartz	07KNSTD	170,865	10,316	23,224	1,410	1,972	24,628
Bedoira 3	44.3291	7.4178	770	std	3	2.65	0.882	2006	Be-10	quartz	07KNSTD	165,818	10,799	24,530	1,607	2,169	26,102
Bedoira landform age (ka)[g]	--	--	--	--	--	--	--	--	--	--	--	--	--	**23,585**	**720**	**1,574**	**25,031**
Festiona 1	44.2986	7.3404	782	std	3	2.65	0.970	2006	Be-10	quartz	07KNSTD	212,728	16,844	28,242*	2,252	2,809	30,381*
Festiona 2	44.2986	7.3394	783	std	3	2.65	0.968	2006	Be-10	quartz	07KNSTD	135,138	4,620	18,344	630	1,257	19,197
Festiona 3	44.2978	7.3376	802	std	3	2.65	0.978	2006	Be-10	quartz	07KNSTD	124,314	16,909	16,496	2,253	2,456	17,196
Festiona 4	44.2985	7.3364	787	std	3	2.65	0.976	2006	Be-10	quartz	07KNSTD	133,362	15,835	17,909	2,136	2,385	18,728
Festiona 5	44.2990	7.3352	780	std	3	2.65	0.947	2006	Be-10	quartz	07KNSTD	141,975	4,761	19,674	663	1,342	20,653
Festiona landform age (ky)[g]	--	--	--	--	--	--	--	--	--	--	--	--	--	**18,837**	**438**	**1,199**	**19,730**
Bergemolo 1	44.2837	7.2918	1,404	std	4	2.65	0.951	2006	Be-10	quartz	07KNSTD	201,878	7,036	16,790*	588	1,155	17,505*
Bergemolo 2	44.2848	7.2886	1,370	std	4	2.65	0.970	2006	Be-10	quartz	07KNSTD	259,293	17,524	21,441	1,457	1,934	22,595
Bergemolo 3	44.2842	7.2891	1,390	std	4	2.65	0.983	2006	Be-10	quartz	07KNSTD	316,317	56,228	25,163	4,501	4,743	26,842
Bergemolo landform age (ka)[g]	--	--	--	--	--	--	--	--	--	--	--	--	--	**21,794**	**1,386**	**1,896**	**22,981**

[a]Determined using handheld GPS.

[b]Combined topographic and self shielding determined over 30° increments using a Brunton compass and clinometer. Dimensionless.

[c]Calculated from $^{10}Be/^{9}Be$ ratios measured at PRIME Lab, Purdue University, against AMS standards in the 07KNSTD series (Nishiizumi et al., 2007). A process blank correction of 19.08 ± 1.729 x 10^{-15} (mean and standard deviation, n=3) was applied to all sample analyses. Uncertainties are reported at 2σ.

[d]Calculated using version 3 of the exposure age calculator formerly kown as the CRONUS-Earth online exposure age calculator (http://hess.ess.washington.edu/). Ages reported here are based on the Lifton-Sato-Dunai scaling (LSDn; Lifton et al., 2014) using a sea level-high latitude (SLHL) reference production rate of 3.92 atoms g⁻

[e]Reflects the uncertainty in AMS measurement, number of atoms of ^{9}Be added via carrier solution, and other uncertainties related to sample preparation. Reported at 2σ.

[f]Reflects both internal (analytical) uncertainty and uncertainty in ^{10}Be production rate and scaling. Reported at 2σ.

[g]Error-weighted mean, one-, and (two)-standard deviation of data after removing outliers using the sumamry statistics function in the online calculator formerly known as the CRONUS-Earth online exposure age calculator (http://hess.ess.washington.edu/). Outliers denoted with a *. See text for details.

Internal uncertainty[e] (yr)	External uncertainty[f] (yr)
1,107	1,921
1,592	2,226
1,827	2,466
814	**1,780**
2,617	3,264
692	1,380
2,452	2,673
2,342	2,615
733	1,484
482	**1,318**
640	1,259
1,625	2,158
5,139	5,415
1,550	**2,124**

[1] yr^{-1} (Brochers et al., 2016).